

Computational Modelling of A Methane Steam Reforming Reactor

by

Andres Alejandro Sola Quiroz

A thesis submitted in partial fulfillment of the requirements for the degree of

Master of Science

In Chemical Engineering

Department of Chemical and Materials Engineering
University of Alberta

© Andres Alejandro Sola Quiroz, 2015

Abstract

The majority of industrial chemical reactors are based on the packed bed reactor. This is the main reason why these types of reactors have been a subject of so many investigations. They are primarily used because of their simplicity at the moment of their design, build and operation (Hayes, 2013). However, at the moment of design, simplicity can carry some lack of accuracy. Depending on the goals of each project this can be acceptable but some other projects demand more certainty of the processes that occur inside the reactor and of the outcome obtained at the outlet of itself. Thus, a more detailed two dimensional modeling methodology is what this investigation aims for.

Based on data obtained from the work of Zeiser et al. (2001) and the experimental work of Benenati et al. (1962), an equation is developed to obtain a variable porosity, which is more realistic compared to the use of a constant porosity over the reactor. The equation is made for an average porosity of 0.38 and a tube to particle diameter ratio of 10.

In this work, a packed bed two dimensional heterogeneous axisymmetric model which includes: mass balances and energy balances for the solid and the fluid phases, Ergun equation to calculate the permeability and account for the porosity influence, dispersion mechanisms for the fluid transport, and a radial variable porosity equation, is carried out using COMSOL multiphysics, a commercial finite elements software.

An important final step to this model is the implementation of look-up tables as showed by Votsmeier (Votsmeier, 2009) to obtain the source terms for the chemical reactions. This, using a one dimensional diffusion model to create the tables and pre-calculate source terms for a range of conditions.

Preface

Part of the research conducted in this thesis was done by A. Fadic in collaboration with Dr. R. E. Hayes and Dr. J. Mmbaga. This part of the research covers from the optimization of the one dimensional diffusion model (to achieve faster convergence) described in Chapter Three, to the creation of the look-up tables containing the source terms of the chemical reactions. The aforementioned work, also includes the reduction of the errors of the look-up tables.

Dr. R. E. Hayes was the supervisory author of this work involved throughout the research with concept formation in theoretical aspects and providing guidance.

To my parents, my sister, and my grandparents...

Acknowledgments

I would like to extend my gratitude to my research supervisor Dr. Robert E. Hayes for his continuous support throughout these years. I feel extremely grateful of him for accepting me under his mentorship and privileged for this learning opportunity.

I would also like to thank Anton Fadic, whose work has not only been of great importance to this thesis, but also with advises, discussions and ideas helped me increase the quality of my research.

I would like to acknowledge Dr. Joseph Mmbaga for his support and patience especially when I was starting to learn CFD; I always knew that I could count with his help if I needed it, which was very reassuring. I would also like to thank him for his kind and pleasant personality.

I would also like to thank my colleagues and friends Libardo Estupinan, Ashwin Kumar and Pedro Mateo for their valuable insights and technical assistance.

Table of Contents

1. Introduction	1
2. Background.....	3
2.1. Introduction	3
2.2. Packed Bed Reactors.....	4
2.2.1. Description of packed beds.....	4
2.2.2. Heat and mass transfer	6
2.2.3. Porosity	9
2.2.4. Packed bed models for mole and energy balances.....	11
2.3. Methane reforming.....	16
2.3.1. Natural gases.....	16
2.3.2. Hydrogen and carbon monoxide production.....	17
2.3.3. Steam reforming.....	19
3. Methodology.....	24
3.1. Introduction	24
3.1.1. Non-isothermal flow	26
3.1.2. Mass balance for fluid.....	28
3.1.3. Mass balance for the solid.....	31
3.1.4. Energy balance for fluid.....	32
3.1.5. Energy balance for solid	34
3.1.6. Radial porosity variation.....	37
3.1.7. Procedure in brief.....	39
3.1.8. Computing the effectiveness factor	39
3.1.9. Look-up tables and errors	43
4. Results and discussion.....	47
4.1.1. Sensitivity analysis.....	56

4.1.2. Case studies.....	58
5. Summary and conclusions.....	60
5.1. Future work	61

List of Tables

<i>Table 1: Types of heat and mass transfer that can affect a packed bed.</i>	<i>8</i>
<i>Table 2: Typical composition of a natural gas with a low concentration of CO₂</i>	<i>16</i>
<i>Table 3: Typical composition of a natural gas with a high concentration of CO₂.....</i>	<i>17</i>
<i>Table 4: the main reactions of Methane Steam Reforming.....</i>	<i>19</i>
<i>Table 5: Others reactions which happen during Methane Steam Reforming.....</i>	<i>20</i>
<i>Table 6: Grid independence analysis</i>	<i>48</i>
<i>Table 7: Results for order of the method, discretization error and exact solution.....</i>	<i>49</i>
<i>Table 8: Comparison of the mole fractions averages over the inlet and the outlet.....</i>	<i>53</i>
<i>Table 9: Results of the sensitivity analysis of parameters of the model with its corresponding variation.....</i>	<i>57</i>
<i>Table 10: Results of case studies with its corresponding variation of parameters of interest</i>	<i>58</i>

List of Figures

<i>Figure 1: Typical radial temperature and concentration profile</i>	7
<i>Figure 2: Heat transfer near a solid-to-solid contact; (Koning, 2002)</i>	9
<i>Figure 3: Radial void fraction distribution for a sphere-packed bed with $DtDp = 10$</i>	10
<i>Figure 4: Geometry of the modeled reactor in a) and b) is a zoom-in of the geometry to visualize the mesh style.</i>	25
<i>Figure 5: Developed equation of radial porosity distribution compared against the results obtained by Zeiser et al. (2001) and Bay et al. (1997).</i>	38
<i>Figure 6: Geometry of one dimensional diffusion model</i>	40
<i>Figure 7: Methane mole fraction, diffusion model</i>	42
<i>Figure 8: Mole fractions (Left) and effective diffusivities (Right), diffusion model</i>	43
<i>Figure 9: Spline function rate errors for methane</i>	45
<i>Figure 10: Spline function rate errors for carbon dioxide</i>	45
<i>Figure 11: Velocity profile, Packed bed reactor model</i>	49
<i>Figure 12: Axial velocity magnitud at the centerline (Left) and radial velocity magnitud at $z = 0.45[m]$</i>	50
<i>Figure 13: Reynolds number evaluated radially at $z = 0.45[m]$</i>	50
<i>Figure 14: Density of the mixture over the reactor geometry</i>	51
<i>Figure 15: Pressure over the reactor geometry</i>	51
<i>Figure 16: Mole fraction of methane over the reactor geometry</i>	52
<i>Figure 17: Axial mole fractions over the center line of the reactor</i>	52
<i>Figure 18: Temperature of the fluid over the reactor geometry</i>	53
<i>Figure 19: Comparison between the temperature of the fluid and the one of the solid.</i>	54
<i>Figure 20: Effectiveness factor over the reactor geometry</i>	54
<i>Figure 21: Reaction rate over the reactor geometry</i>	55
<i>Figure 22: Radia reaction rate evaluated at the outlet</i>	55

Nomenclature

U	Overall heat transfer coefficient
h_w	Wall heat transfer coefficient
$h_{w,eff}$	Effective wall heat transfer coefficient
k_r	Radial thermal conductivity
k_a	Axial thermal conductivity
$k_{r,eff}$	Effective radial thermal conductivity
$k_{a,eff}$	Effective axial thermal conductivity
D_t	Tube (reactor) diameter
ϕ	Porosity
v_s	Superficial velocity
v	Interstitial velocity
z	Axial direction
r	Radial direction
P	Pressure
D_p	The equivalent particle diameter
ρ	Density
μ	Dynamic viscosity
Re_b	Reynolds number of the bed $\frac{D_p \rho v_s}{\mu}$
R_g	The gas constant

M_i	Molar weight of the i-th molecule
T_f	Fluid temperature
ΔF_A	Molar flow rate variation of the reactant A in the control volume
η	Effectiveness factor
R_A	Rate of disappearance of A
ρ_b	Bulk density defined as the catalyst mass divided by the reactor volume
A_c	Cross sectional area
Q_V	Volumetric flow rate
C_P	Heat capacity dependent of composition and temperature
ΔH_R	The enthalpy change of reaction
$v_s \rho$	Constant and is equal to the superficial mass velocity G
$F_{A,f}$	The molar flow rate of the reactant A in the fluid phase
k_m	The mass transfer coefficient
ΔS	The external catalyst surface inside of the control volume
C_f	The total molar concentration in the fluid phase
$Y_{A,f}$	The molar fraction of A in the fluid phase and
$Y_{A,s}$	The molar fraction of A in the solid phase
a_m	The effective area for mass transfer, defined as the particle surface area divided by bed volume

ρ_C	The catalyst density defined as mass of a catalyst particle divided by the volume of a catalyst particle
ΔT_f	the variation of the temperature of the fluid phase
h_{fs}	the fluid-solid heat transfer coefficient
T_S	the temperature of the solid
T_f	the temperature of the fluid
T_b	the temperature of the bed
T_w	the temperature of the wall
T_0	Bed inlet temperature
D_T	the reactor diameter ($\pi D_T \Delta z$ accounts for the external area of the tube)
$T_{3,\infty}$	the external fluid temperature, surrounding the reactor
D_{ea}	the dispersion coefficient for axial flow
k_{af}	Axial fluid thermal conductivity
k_{as}	Axial solid phase thermal conductivity
D_{er}	Radial dispersion coefficient
h_{fs}	Fluid-solid heat transfer coefficient
h_{wf}	Wall-fluid heat transfer coefficient
h_{ws}	Wall-solid heat transfer coefficient
R_i	Reaction rate in $\text{mol m}^{-3}\text{s}^{-1}$
ε	Porosity, only in Section 3.1.8

τ	Tortuosity, only in Section 3.1.8
D_p	Diameter of a spherical particle (m)
D_t	Diameter of the tube (m)
D_{pv}	Diameter of equivalent-volume sphere (m)
ϕ	Bed void fraction, porosity
$(-R_A)_s$	The reaction rate of the specie A evaluated at surface conditions
ρ_b	The bulk density defined as the catalyst mass divided by the reactor volume
j_D	Dimensionless mass transfer factor for gases
j_H	Dimensionless heat transfer factor for gases
Sc	$\frac{\mu}{\rho D}$, Schmidt number
Pr	$\frac{c_p \mu}{k_f}$, Prandtl number
Nu	$\frac{h_{fs} D_p}{k_f}$, Nusselt number
D_B	Hydraulic diameter
Sh	Sherwood number
k_f	Thermal conductivity of the fluid
k_p	Thermal conductivity of the solid
k_{rf}	Radial fluid thermal conductivity
D_T	Tube diameter

D_p	Particle diameter
k_{rs}	Radial conductivity of the solid
k_{as}	Axial conductivity of the solid
C_p	Heat capacity at constant pressure
c_s	Solid specific heat
\dot{m}_f	Superficial fluid mass velocity
R	Tube radius
t	Time
η	Effectiveness factor
Pe_a	Effective axial Peclet number $\frac{\dot{m}_f c_f D_p}{k_a}$
Pe_r	Effective radial Peclet number $\frac{\dot{m}_f c_f D_p}{k_r}$
$(Pe_m)_r$	Radial Peclet number for mass transfer
$(Pe_m)_a$	Axial Peclet number for mass transfer
D	Molecular diffusion average
D_{im}	Molecular diffusion of i
μ_f	Dynamic viscosity of a gas mixture
u	Velocity vector, radial velocity when indicated
$\omega_{i,fluid}$	Mass fraction in the fluid of i
$\omega_{i,solid}$	Mass fraction in the solid of i

D_{iK}	Knudsen diffusion of the i-th component
----------	---

Chapter 1

1. Introduction

Among the numerous types of chemical reactors existing in the world, one of the most important ones is the packed bed reactor. The majority of industrial chemical reactors are based on the fixed bed concept. Synthesis of methanol, steam reforming of natural gas, and the synthesis of ammonia from hydrogen and nitrogen are some of its most known uses in industry.

Steam reforming is the reaction between steam and hydrocarbons to give a mixture of hydrogen, carbon monoxide, methane and steam. The reforming reaction involving two stable molecules such as methane and water is strongly endothermic and it leads to the formation of more molecules. The positive heat of reaction of the reforming reaction and the high exit temperatures at typical process conditions mean that heat must be supplied to the process typically in a fired tubular reactor. This process is a key technology for the manufacture of synthesis gas and hydrogen.

In this work, a packed bed two dimensional heterogeneous axisymmetric model which includes: mass balances and energy balances for the solid and the fluid phases, Ergun equation to calculate for the permeability, volume forces to account for the porosity influence, and dispersion mechanisms for the fluid transport, is carried out using COMSOL multiphysics, a commercial finite elements software.

The objective of this work was to develop a detailed two dimensional packed bed reactor model for steam methane reforming and to study the effect of how the change on important parameters and some boundary conditions affect the conversions of reactants and the model in general. Of great interest is the porosity variation in a packed bed reactor. Literature shows that porosity varies inside the reactor and that it increases considerably in the areas near the wall. Most reactor modellings does not include this effect, which can be significant in small diameter reactors. A study is done to account for the porosity. Also, a sophisticated manner of accounting for reaction kinetics is applied thanks to the use of look up tables.

In this thesis, Chapter 2 gives a review of the background of packed beds, including a general description, some characteristics of the behavior of heat and mass transfer, porosity and some models that have been used to describe it. There is also a review of background for methane steam reforming. Showing a general description, its stoichiometric behavior, and global kinetics found in literature.

Chapter 3 contains a description of the methodology used to build the packed bed reactor model for methane steam reforming, the boundary conditions used, the initial values, the methods used to include the properties of the components and all of the equations and the modules of the computational package used to do the simulations.

Chapter 4 shows the results obtained from the main model developed, a sensitivity analysis to how some of the internal parameters of the model affect the results and some study cases of how the model behaves when changing some boundary conditions. There is also a discussion of the important results obtained and of the variation of the results from the different analysis.

Chapter 5 presents the main conclusions obtained from the work and the studies developed, and also of the opportunities for future work in this area.

Chapter 2

2. Background

2.1. Introduction

Packed bed reactors are widely used in industry and from there comes its importance. Figuring out and understanding all of its behavior can help improve the modeling and functioning of this kind of reactors, principally by reducing the malfunctioning and improving its performance, which will only happen as knowledge of its characteristics increase.

This Chapter consist of two parts, the first one is related with a description of the reactor, and the second part deals with natural gas steam reforming.

For the first part of this chapter, a general study of the packed bed reactor is done. A description of its main characteristics is commented along with the general mathematical models that help to predict the behavior of the reactor. Some of its sub-models are also showed, these last are more related with the parameters that the general model use, and how to obtain more exact values for them.

For the second part of this chapter, a general study of methane reforming is made. Methane reforming is the most widely used process to produce syngas because of the wide availability and low price of natural gas. The hydrogen which is produced is a high-value product which can be used as a reactant in the petrochemical industry to produce methanol, ammonia or even hydrocarbons through the Fischer-Tropsch synthesis, which will be further blended into diesel.

Among the four possible ways to produce hydrogen from natural gas, the two most broadly commercialized used are: Steam Reforming and Dry Reforming. Only steam reforming is discussed in this thesis.

2.2. Packed Bed Reactors

2.2.1. Description of packed beds

The packed bed reactor is one of the most widely used reactors in industry for the synthesis of large-scale chemicals. It uses heterogeneously catalyzed fluid reactions that occur on the surface of solid catalyst particles. This leads to diverse and meaningful properties of the reactor such as the bed porosity or the conversion of the reactor, which will differentiate one packed bed reactor from another. Moreover, packed bed reactors have been very useful when it comes to manage toxic and harmful substances. One example is the application of fixed beds for the purification of combustion exhaust.

Depending on the final use of a packed bed reactor, different configurations and set ups will be used. One of the most important differentiations of packed beds is whether or not it operates adiabatically. The effects that temperature produce on a chemical reaction and the election of the kind of reactor to use will depend on the magnitude of the reaction enthalpy variation. When there is a small enthalpy variation an adiabatic reactor should be used. The general idea is that the adiabatic temperature development will not affect negatively on the selectivity or the yield. An adiabatic reactor can be described as a uniformly distributed set of catalytic particles covered by an (usually tubular) outer insulated container.

On the other hand, when there is a large enthalpy variation or when a reaction is very sensitive to temperature a non-adiabatic reactor would be recommendable to use along with a heat exchanger integrated with the bed (there can be other options to solve the problem). For the case of big enthalpy changes, there are two risks that have to be managed: that if the temperature is constantly reduced due to an endothermic reaction it can reduce the rate of reaction significantly, and that if temperature constantly increase due to an exothermic reaction the reactor can be damaged (Hayes & Mmbaga, 2012). Both cases can be managed very well using a non-adiabatic reactor.

It is worth to mention, that for adiabatic reactors the diameter of the reactor typically does not have a lot of impact on its operation. However, for a non-adiabatic reactor with external heat exchange, the diameter of the reactor becomes a very important factor and to favor heat exchange the diameter must be relatively small, often around 10 particle diameters (Hayes & Mmbaga, 2012). Because of this reactor diameter restriction (due to a fairly small thermal conductivity of the packed beds),

a widely used arrangement for non-adiabatic reactors is the multi-tubular packed bed reactor, in which multiple reactors are placed in parallel inside of a large vessel. Heat transfer fluid flows over the tubes creating in effect a large heat exchanger.

Industrially, most packed bed reactors are operated under constant operating conditions. Because of this, all of the industry efforts aim to achieve the optimum stationary reactor performance. However, it is very important to study all kinds of behaviors of the packed bed reactors, either stationary or non-stationary. Because of its wide use on industry, the knowledge about its different behaviors is highly valued to improve the operation and control to be able to maximize the conversion (among others) and to minimize the costs.

Some of the general many advantages that the use of packed bed provides are its high conversion per unit mass of catalyst, its low operating costs, the possibility of continuous operation, stability on its operation conditions, no moving parts to wear out, catalysts stay in the reactor, easy separation of the mixture and the catalysts if necessary, relatively easy design depending on the needs, effective at high temperatures and pressures, and minimum product inhibition when compared to stirred tank reactors.

Some of the general disadvantages when using packed beds are that the temperature control can be challenging, channeling may occur, there can exist undesired thermal gradients, its difficulty for service and clean and undesirable side reactions.

Among the several gas-solid catalyzed reactions utilized commercially one can highlight the steam reforming of natural gas and naphtha, the oxidation of ethylene, c4 hydrocarbons, benzene and methanol, the hydro chlorination of methanol, the ammoxidation of propylene and methanol synthesis.

2.2.2. Heat and mass transfer

Fixed bed reactors contain catalyst pellets that can have different shapes and that are usually placed randomly inside of the reactor. Most of the time, the mass velocity in the bed is bigger than 1 kilogram per square meter of reactor cross section per second, which produces enough turbulence to make the transport resistance in the catalyst pores large compared with the gas-catalyst mass transfer resistance (Eigenberger & Ullmann, 1992). One of the many assumptions used to model this kind of reactors is that the entire surface of the catalyst particle is equally exposed to uniform concentration and temperature of the flow. However, this rarely happens on random packing. Most packed bed reactor models use volumetrically averaged values of the variables of interest, which is often sufficiently accurate for design work. In this manner, the models for packed bed reactors can supply reliable information. It is very difficult to differentiate when measuring gas temperature and catalyst temperatures. This is the principal reason why the quasi-homogeneous model is the most frequently used when it comes to execute design and simulation predictions, where a single temperature is used to describe both the fluid and solid phases.

For two dimensional models, the main assumption made is axial symmetry, meaning that the reactor being represented would not have porosity variations in the angular direction. There are two important zones of the reactor that have to be considered: the wall zone and the core zone. With an exothermic reaction, a parabolic shaped profile typically represents the behavior of the temperature on the core zone as can be seen in Figure 1. However, in the wall zone the profile tends to be a sharp decrease (Koning, 2002).

The heat flux at the wall will be proportional to the temperature difference between the wall and the fluid near the wall. This proportionality coefficient is called the wall heat transfer coefficient h_w . The radial mass flux at the wall is equal to zero, since most of the time the wall is assumed to be impermeable.

The radial heat flux in the packing can be assumed to have the characteristics of solids and stagnant fluids, thus Fourier's law for conduction is widely used.

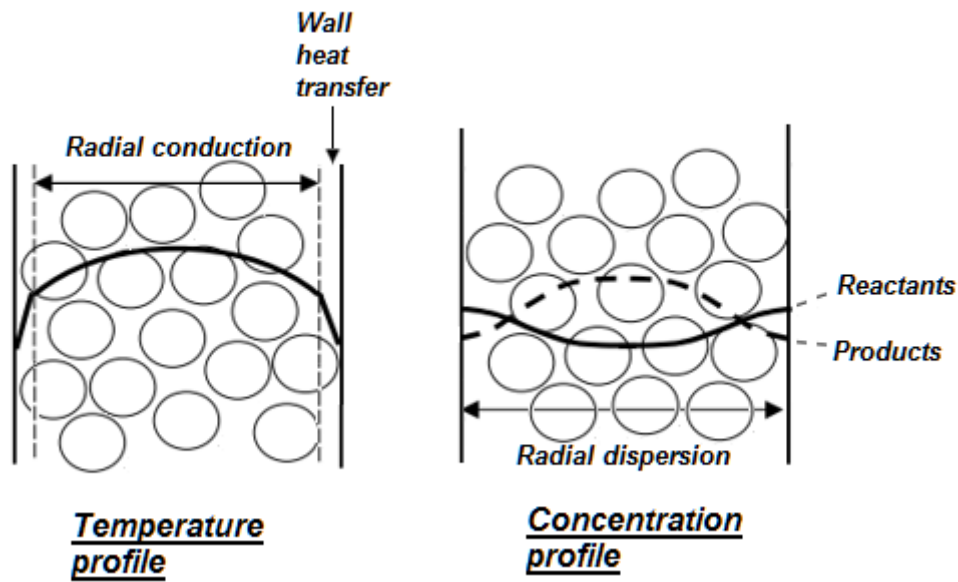


Figure 1: Typical radial temperature and concentration profile; based on Koning, 2002

For the radial mass flux in the packing, usually the dominant form of transport is by dispersion, in this cases Fick's law of molecular diffusion can be used (Koning, 2002).

Convection and mixing are usually the main causes of dispersion in packed beds, and this dispersion is what makes it necessary to replace the thermal conductivity by an effective thermal conductivity and the diffusion coefficient by an effective diffusion coefficient. These effective parameters will be affected by geometry of the catalyst particles, geometry of the reactor, operating conditions and physical properties. Additional dispersion can be added when dealing with variation in the fluid density (Benneker, Kronberg, Post, Ham, & Westerterp, 1996).

According to Koning (2002) there are many different kinds of heat and mass transfer parameters that can affect the performance of a packed bed. These effects are summarized in Table 1.

Table 1: Types of heat and mass transfer that can affect a packed bed.

Independent of Fluid Velocity	Dependent on Fluid Velocity
Conduction/diffusion through the solid	Convection by the fluid in axial direction
Conduction through solid-solid contact points	Axial and transverse mixing of the fluid
Heat transfer by radiation between surfaces	Fluid-solid heat and mass transfer
Diffusion and conduction within the fluid	Diffusion and conduction through fluid film near solid-solid contact points

In these reactors, mixing is assisted by turbulence and molecular diffusion.

Gradients of temperature or concentration between the fluid and the solid will promote the mass and heat transfer. Moreover, if a chemical reaction happens inside of a catalyst particle a temperature profile will appear within the particle. In the same manner, because reactants are being consumed and products are being formed, concentration gradients will also appear within the particle. Usually porous catalyst particles have thermal conductivities between 0.5 and 2 $\text{Wm}^{-1}\text{K}^{-1}$ and the variations in the temperatures inside of the particles are most of the times small. Thus, for the calculation of reaction rates the thermal conductivity can be assumed to be constant.

Two of the most important design parameters, the effective radial heat transfer coefficient and the wall heat transfer coefficient, decrease when decreasing the particle size. When increasing the particle size the concentration of the reactant will decrease towards the center of the particle and it will decrease the reaction rate per unit volume of catalyst (Koning, 2002).

In contrast to the effect of particles mass transport to the overall mass transport in the reactor, the heat transport through the catalyst particles might be meaningful to the overall radial and axial heat transport if its thermal conductivity and the fluid velocity allow it.

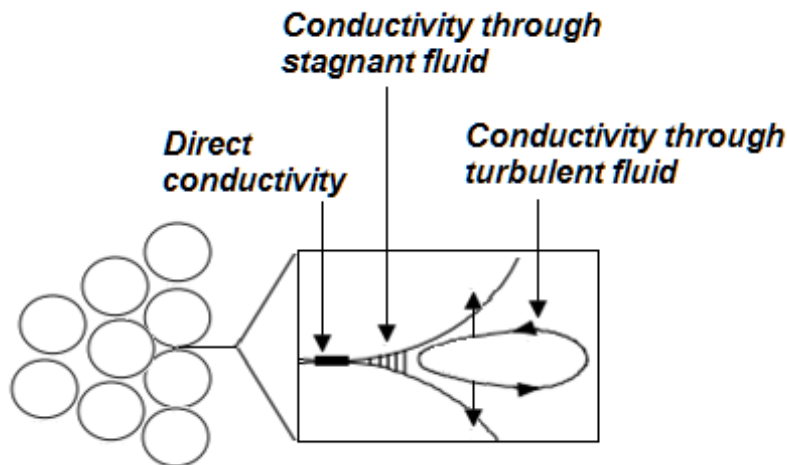


Figure 2: Heat transfer near a solid-to-solid contact; Based on Koning, 2002.

Between two particles there can be 3 types of heat transfer as shown in Figure 2; in the contact area there is solid to solid conduction, then in the (more or less) stagnant fluid area there is conduction from the solid to the fluid to the solid and then moving further from the contact area the heat transfer start to depend more and more in the fluid velocity. Contact area between particles is very hard to measure because it will depend on the form of the particles, on the roughness and the orientation. Radiation will be negligible for temperatures below 400 degrees Celsius (Koning, 2002). The principal difference between the heat transport that happens close to the walls and the one that happens in the packing is that the particles and the fluid will interchange heat with the walls as well, which can be taken as a flat surface compared with the particles and it also can have a constant and uniform temperature. To account for this physical difference and the steep gradient that it produces, the use of a wall heat transfer coefficient is present in most models.

2.2.3. Porosity

The porosity is the void space in the reactor through which the gas mixture can flow. It is measured as the void volume divided by the reactor volume (Hayes & Mmbaga, 2012).

In packed beds, it is well documented that in the vicinity of the tube wall the void fraction nears unity (Benenati & Brosilow, 1962; Bey & Eigenberger, 1997) creating a channeling effect. Studies

have shown that radial inhomogeneities have to be properly considered for the radial heat transfer and reaction to be modelled correctly (Bey & Eigenberger, 1997).

Different kinds of studies and experimental techniques have been carried out to measure the void fraction of packed beds. Benenati et al. (Benenati & Brosilow, 1962) poured into a container uniformly sized spherical pellets and then filled the void space with a liquid epoxy resin. They allowed it to cure for 100 hours. The solid final cylinder was turned down to smaller diameters progressively using a machinist's lathe until a bed diameter of 0.75 inches was reached (minimum before breaking the bed). They calculated an average porosity for every diameter segment taken out of the solid resin cylinder to obtain an experimental radial dependent porosity for the full bed.

In another study, Zeiser et al. (Zeiser et al., 2001) used a Computational Fluid Dynamics (CFD) calculation to investigate the flow field, dispersion and reaction in a packed bed. For the development of their model, they created the geometry of random packing inside a tube synthetically by means of a Monte-Carlo simulation. They compared the void fraction radial distribution that they found with the curve obtained by Bey and Eigenberger (Bey & Eigenberger, 1997) from their correlation developed by fitting experimental data. This was for a packed bed with $D_t/D_p = 10$ (tube to particle diameter ratio) and both curves can be compared in Figure 3, which shows porosity “ ε ” against dimensionless distance from the wall (in number of particle radius).

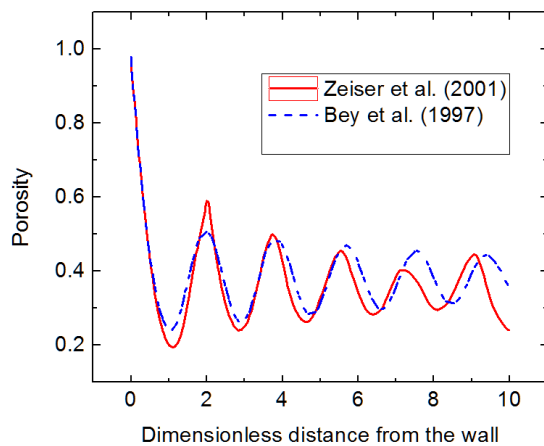


Figure 3: Radial void fraction distribution for a sphere-packed bed with $D_t/D_p = 10$

2.2.4. Packed bed models for mole and energy balances

There are multiple models that represent the behavior of packed beds. The selection of one of them depends on time, computational resources available and accuracy needed.

In literature, lots of models can be found. One dimensional or two dimensional, adiabatic or non-adiabatic, plug flow models, dispersion models, pseudo-homogeneous or heterogeneous, among others.

For this work, a two dimensional heterogeneous steady state model was elected as the main model to use. This is because it is a more realistic model than most of the other options and because even though there might be other more accurate models (for example three dimensional models), this one is computationally feasible taking into account the available resources and it allows us to include porosity variations.

Heterogeneous model means that the model differentiates between the solid part of the reactor and the fluid part. Being a two dimensional model means that for some coefficients there is an axial and a radial component that will vary.

This is a dispersion model, therefore it uses a dispersion coefficient in the mole balances where other models use a diffusion coefficient and its value does not depend on the type of species (Hayes & Mmbaga, 2012).

Mole balance for the fluid

The mole balance for the fluid phase in cylindrical coordinates can be written:

$$\frac{1}{r} \frac{\partial}{\partial r} \left(r D_{er} C_f \frac{\partial Y_{A,f}}{\partial r} \right) + \frac{\partial}{\partial z} \left(D_{ea} C_f \frac{\partial Y_{A,f}}{\partial z} \right) - C_f v_s^* \frac{\partial Y_{A,f}}{\partial z} - k_m a_m C_f (Y_{A,f} - Y_{A,s}) = 0 \quad (1)$$

With a_m as the total catalyst external surface area divided by the volume of the reactor, r as the radial direction, z as the axial direction, D_{er} as the dispersion in the radial direction, D_{ea} as the dispersion in the axial direction, C_f as the total concentration in the fluid, $Y_{A,f}$ as the mole fraction of the specie A in the fluid, v_s as the superficial velocity and k_m as the mass transfer coefficient.

Mole balance for the solid

The mole balance for the solid equates the rate of reaction in the solid to the rate of mass transfer from the fluid.

$$k_m a_m C_f (Y_{A,f} - Y_{A,S}) - \eta (-R_A)_S \rho_b = 0 \quad (2)$$

With η as the effectiveness factor, $(-R_A)_S$ as the reaction rate of the specie A evaluated at surface conditions and ρ_b as the bulk density defined as the catalyst mass divided by the reactor volume.

Energy balance for the fluid

The fluid phase energy balance in cylindrical coordinates is:

$$\frac{1}{r} \frac{\partial}{\partial r} \left(k_{rf} \frac{\partial T_f}{\partial r} \right) + \frac{\partial}{\partial z} \left(k_{af} \frac{\partial T_f}{\partial z} \right) - v_s \rho C_p \frac{\partial T_f}{\partial z} - h_{fs} a_m (T_f - T_S) = 0 \quad (3)$$

With k_{rf} as the radial thermal conductivity of the fluid, k_{af} as the axial thermal conductivity of the fluid, T_f as the temperature of the fluid, T_S as the temperature of the solid, ρ as the density of the fluid, C_p as the heat capacity of the fluid at constant pressure, and h_{fs} as the fluid-solid heat transfer coefficient.

For this equation it is necessary to know the values for the axial and radial thermal conductivities of the fluid.

Energy balance for the solid

$$\frac{1}{r} \frac{\partial}{\partial r} \left(k_{rs} \frac{\partial T_S}{\partial r} \right) + \frac{\partial}{\partial z} \left(k_{as} \frac{\partial T_S}{\partial z} \right) - \Delta H_R \eta (-R_A)_S \rho_b - h_{fs} a_m (T_f - T_S) = 0 \quad (4)$$

With k_{rs} as the radial thermal conductivity of the solid and k_{as} as the axial thermal conductivity of the solid.

For this equation it is necessary to know in advance the values for the axial and radial thermal conductivities of the solid.

Momentum balance and continuity equation

For the momentum balance a volume-averaged Navier-Stokes equation can be used. For the packed bed an expression for the permeability K is needed. Volume forces can be set to account for the porosity. Its implementation is shown in Chapter 3.

$$\rho(u \cdot \nabla)u = \nabla \cdot \left[-pI + \mu(\nabla u + (\nabla u)^T) - \frac{2}{3}\mu(\nabla \cdot u)I \right] + F \quad (5)$$

$$\nabla \cdot (\rho u) = 0 \quad (6)$$

With u as the velocity, p as the pressure, μ as the viscosity, I as the identity matrix and F in this case as the volume forces.

Boundary conditions

The boundary conditions are given in the following.

For the inlet when using an inlet extension region before the packed bed.

For the mole balance, the mole fractions of the used species must be known in the inlet and they are constants:

$$Y_{A,fo} = Y_{A,f} \text{ at } z = 0 \quad (7)$$

For the energy balance of the fluid a constant temperature is set at the inlet:

$$T_{fo} = T_f \text{ at } z = 0 \quad (8)$$

For the energy balance of the solid no axial variation of the temperature at the inlet:

$$\frac{\partial T_S}{\partial z} = 0 \text{ at } z = 0 \quad (9)$$

For the momentum balance a constant normal velocity is set in the inlet

$$v = v_0 \text{ at } z = 0 \quad (10)$$

For the reactor outlet

For the mole balances and the energy balances

$$\frac{\partial Y_{A,f}}{\partial z} = \frac{\partial T_f}{\partial z} = \frac{\partial T_s}{\partial z} = 0 \quad \text{at } z = L \quad (11)$$

And for the momentum balance

$$p = p_0 \quad \text{at } z = L \quad (\text{pressure, no viscous stress}) \quad (12)$$

For the centerline

$$\frac{\partial Y_{A,f}}{\partial r} = \frac{\partial T_f}{\partial r} = \frac{\partial T_s}{\partial r} = \frac{\partial u_r}{\partial r} = 0 \quad \text{at } r = 0 \quad (13)$$

With u_r as the radial component of the velocity

For the wall

For the reactor wall mole balance:

$$\frac{\partial Y_{A,f}}{\partial r} = 0 \quad \text{at } r = R \quad (14)$$

For the momentum balance

$$\frac{\partial u_r}{\partial r} = 0 \quad \text{at } r = R \quad (\text{slip condition}) \quad (15)$$

For an adiabatic reactor wall energy balance:

$$\frac{\partial T_f}{\partial r} = \frac{\partial T_s}{\partial r} = 0 \quad \text{at } r = R \quad (16)$$

For an adiabatic reactor wall energy balance

For the fluid:

$$-k_{rf} \frac{\partial T_f}{\partial r} = U_f (T_f - T_{3,\infty}) \quad \text{at } r = R \quad (17)$$

For the solid:

$$-k_{rs} \frac{\partial T_s}{\partial r} = U_s (T_s - T_{3,\infty}) \quad \text{at } r = R \quad (18)$$

Many equations have been proposed for the overall heat transfer coefficient U and the same equation can be used to calculate both, U_f and U_s . In this case, for any equation selected, the important thing is to make U_f depend of a wall-fluid heat transfer coefficient h_{wf} and U_s to depend of a wall-fluid heat transfer coefficient h_{ws} instead. In equations 17 and 18, $T_{3,\infty}$ is the external fluid temperature that surrounds the reactor.

The sub-models for the parameters are described in Chapter 3.

2.3. Methane reforming

2.3.1. Natural gases

The term natural gas refers to a hydrocarbon rich gas mixture which comes from the interaction of decomposed plants and animals with landfill gases in underground reservoirs. This can be described as anaerobic decomposition of organic materials. Natural gas is mainly composed of methane (CH₄) mixed with a lower and variable amount of other hydrocarbon gases such as ethane, propane and butane. Carbon dioxide, nitrogen and hydrogen sulfide can also be found in relatively low quantities. Table 2 shows the composition of a certain natural gas containing a low amount of CO₂.

This kind of composition will rather be used for Methane Steam Reforming whereas the natural gas composition presented in Table 3 is ideal for Dry Methane Reforming because of its high concentration in CO₂. Al-Megeren and Xiao (Al-Megeren & Xiao, 2012), state that the concentration of non-hydrocarbon gases corresponding to CO₂, N₂ and H₂S varies between 1% to 99% in natural gas.

Table 2: Typical composition of a natural gas with a low concentration of CO₂

Component	Volume percentage %
Methane, CH ₄	96.0
Ethane, C ₂ H ₆	2.35
Nitrogen, N ₂	0.57
Carbon dioxide, CO ₂	1.08

Based on information from (Al-Megeren & Xiao, 2012)

Table 3: Typical composition of a natural gas with a high concentration of CO₂

Component	Volume percentage%
Carbon dioxide, CO ₂	71
Methane, CH ₄ + Ethane, C ₂ H ₆	28
H ₂ S	0.5
Nitrogen, N ₂	0.5

Based on information from (Richardson & Paripatyadar, 1990)

Although it is a non-renewable resource, natural gas is present in gigantic quantities, especially in Russia and in the United States whose reserves are estimated to be more than 280 million cubic feet, on top of potential more 850 trillion cubic feet.

2.3.2. Hydrogen and carbon monoxide production

In addition to being used as a fuel for domestic and industrial heating or as a transportation fuel, natural gas is also commonly used to produce hydrogen through reforming. Its extraction and transformation into hydrogen has never stopped increasing. For example, 50 million metric tons of hydrogen were produced worldwide in 2005 and this production has increased by approximately 10 % each year since then.

With the wide availability and low historical price of natural gases, steam methane reforming has been the most efficient and widely used large-scale process to produce synthetic gas such as hydrogen (H₂) and carbon monoxide (CO) which are used in different applications. Hydrogen is a high-value product and one of the most important reactants in the chemical and petrochemical industry.

One application of synthesis gas is the Fischer-Tropsch synthesis, which uses hydrogen and carbon dioxide as feedstock with a H₂: CO ratio of 2 to produce liquids. The overall equation of this process is:



Hydrogen is a key reactant in methanol and ammonia synthesis, two important industrial chemicals. Ammonia is an essential compound used for the manufacture of fertilizers and is widely used in many other organic reactions and syntheses of pharmaceuticals. Methanol is one of the most abundant chemical commodities in the world as it is used as an anti-freeze, a solvent and can be blended in gasoline or used as an alternative fuel.

Hydrogen is not only an intermediate in synthesis but is also an energy carrier. Although it is not an energy source, it is abundantly produced by methane reforming and many other processes like liquid hydrocarbon steam reforming, water electrolysis, biomass transformation, among others.

There are four widely used methods to reform methane: Steam Reforming, Dry Reforming, Autothermal Reforming and Partial Oxidation, which all have different products distribution, kinetics and thermodynamics. In this work, only the first one is discussed: Steam Reforming which can also be referred as H₂O reforming.

2.3.3. Steam reforming

Steam reforming refers to the reaction of methane with water, and is the most common industrial route for the manufacture of syngas.

2.3.3.1. Reactions

Steam reforming consists of two overall reactions: the steam reforming reaction (I) and the water-gas-shift reaction (II).

Table 4: the main reactions of Methane Steam Reforming

Reactions	Rate constant expression	Enthalpy of reaction
$\text{CH}_4 + \text{H}_2\text{O} \leftrightarrow \text{CO} + 3 \text{H}_2$ (I) (steam reforming)	$1.198 * 10^{17} e^{-\frac{26830}{T}}$	$\Delta H_{298} = 206 \text{ kJ} \cdot \text{mol}^{-1}$
$\text{CO} + \text{H}_2\text{O} \leftrightarrow \text{CO}_2 + \text{H}_2$ (II) (water-gas shift reaction)	$1.767 * 10^{-2} e^{\frac{4400}{T}}$	$\Delta H_{298} = -41 \text{ kJ} \cdot \text{mol}^{-1}$

These are not the only reactions which can occur during methane steam reforming, but they are certainly those who contribute the most to the kinetics. There are some other reactions which may occur, which are given in Table 5

Table 5: Others reactions which happen during Methane Steam Reforming

Secondary Reactions	
$\text{CH}_4 + \text{CO}_2 \leftrightarrow 2\text{CO} + 2\text{H}_2$	(III)
$\text{CH}_4 + 3\text{CO}_2 \leftrightarrow 4\text{CO} + 2\text{H}_2\text{O}$	(IV)
$\text{CH}_4 \leftrightarrow \text{C} + 2\text{H}_2$	(V) (Methane decomposition)
$2\text{CO} \leftrightarrow \text{C} + \text{CO}_2$	(VI) (Boudouard reaction)
$\text{CO} + \text{H}_2 \leftrightarrow \text{C} + \text{H}_2\text{O}$	(VII)
$2\text{H}_2 + \text{CO}_2 \leftrightarrow \text{C} + 2\text{H}_2\text{O}$	(VIII)
$\text{CH}_4 + 2\text{CO} \leftrightarrow 3\text{C} + 2\text{H}_2\text{O}$	(IX)
$\text{CH}_4 + \text{CO}_2 \leftrightarrow 2\text{C} + 2\text{H}_2\text{O}$	(X)

Source: (Hou & Hughes, 2001)

2.3.3.2. Effect of temperature, pressure and steam/methane ratio

The endothermic nature of reaction (I) and the volume expansion caused by a more important number of gas moles in the product phase than in the reactant phase require running the reactions at high temperature, above 500°C and low pressure. The industry performs Steam Reforming using temperatures between 800°C to 900°C to react most of the methane. At these operating conditions, the main product of steam reforming is carbon dioxide, CO₂, which is then converted into carbon monoxide, CO, by the inverse water-gas shift reaction, favored at high temperature. Because all these reactions reach equilibrium, the final mixture is made of carbon dioxide, carbon monoxide, hydrogen, methane and steam.

At the inlet of the reformer, reactions I and II have not produced enough hydrogen to prevent the methane decomposition reaction from happening (reaction V in table 5). Indeed, catalysts which

are present in the upper part of the reactor will be prone to coking and it is recommended to keep a temperature low enough, around 550°C, at the bed inlet to minimize this reaction. However, the temperature must be high enough down the reactor to ensure the production of enough hydrogen (from reactions I and II) that will reverse the coking reaction and hinder coke deposition on the catalysts.

It has been found that the H₂O:CH₄ ratio has a great influence on the methane conversion. In fact, the higher its value, the higher the yield that can be reached and lower amount of CO is produced. This phenomena can be explained by the fact that steam hinders the formation of carbon on the catalyst bed.

Generally, a steam-to-methane ratio between 2 and 6 is used in industrial processes. Q. Ming et al. (Ming, Healey, Allen, & Irving, 2002) observed that a nearly total conversion of methane was obtained by using a steam-to-methane ratio of 3 and a temperature of 750°C at the atmospheric pressure.

2.3.3.3. Kinetics

Haberman and Young (Haberman & Young, 2004) used the two main chemical reactions (water gas shift reaction and methane reforming reaction) for their investigation.



With k_{sf} and k_{rf} as the forward reaction rate constants for each reaction. The rate constants for the reverse reactions were obtained from the equilibrium constants,

$$K_{ps} = \frac{k_{sf}}{k_{sb}} = \frac{p_{\text{H}_2} p_{\text{CO}_2}}{p_{\text{H}_2\text{O}} p_{\text{CO}}} = \frac{X_{\text{H}_2} X_{\text{CO}_2}}{X_{\text{H}_2\text{O}} X_{\text{CO}}} \quad (21)$$

$$K_{pr} = \frac{k_{rf}}{k_{rb}} = \frac{p_{\text{CO}} p_{\text{H}_2}^3}{p_{\text{CH}_4} p_{\text{H}_2\text{O}}} = \frac{X_{\text{CO}} X_{\text{H}_2}^3 p^2}{X_{\text{CH}_4} X_{\text{H}_2\text{O}}} \quad (22)$$

These equilibrium constants can be found as temperature dependent equations (Twig, 1989),

$$K_{ps} = \exp(-0.2935Z^3 + 0.6351Z^2 + 4.1788Z + 0.3169) \quad (23)$$

$$K_{pr} = 1.0267 \times 10^{10} \times \exp(-0.2513Z^4 + 0.3665Z^3 + 0.5810Z^2 - 27.134Z + 3.277) \text{ Pa}^2 \quad (24)$$

$$Z = \frac{1000}{T(K)} - 1 \quad (25)$$

Haberman and Young (Haberman & Young, 2004) compared literature rate data for the reactions catalyzed by nickel. They considered the data of two studies and compared the effect of temperature on the production rate of hydrogen for the two reactions (Lehnert, Meusinger, & Thom, 2000; Xu & Froment, 1989). They concluded that the two studies had some quantitative differences, but overall a good qualitative agreement. The quantitative differences were mostly at higher temperatures (over 1150 [K]). From here they picked Lehnert et al. data (Drescher, Lehnert, & Meusinger, 1998; Lehnert et al., 2000).

The final rate equations for the two reactions can be written.

Water gas shift reaction

$$S_{s,H_2} = k_{sf} \left(p_{H_2O} p_{CO} - \frac{p_{H_2} p_{CO_2}}{K_{ps}} \right) \text{ mol m}^{-3} \text{ s}^{-1} \quad (26)$$

$$k_{sf} = 0.0171 \exp\left(-\frac{103191}{RT}\right) \text{ mol m}^{-3} \text{ Pa}^{-2} \text{ s}^{-1} \quad (27)$$

Steam reforming of methane

$$S_{r,H_2} = k_{rf} \left(p_{CH_4} p_{H_2O} - \frac{p_{H_2}^3 p_{CO}}{K_{pr}} \right) \text{ mol m}^{-3} \text{ s}^{-1} \quad (28)$$

$$k_{rf} = 2395 \exp\left(-\frac{231266}{RT}\right) \text{ mol m}^{-3} \text{ Pa}^{-2} \text{ s}^{-1} \quad (29)$$

With R as the universal gas constant $J \text{ mol}^{-1} \text{ K}^{-1}$.

From now S_{s,H_2} will be called “ rws ” and S_{r,H_2} will be called “ rsr ” for simplicity.

With the information above the net rates of production of each species can be written

$$R_{CH_4} = -rsr \quad ; \text{ in mol m}^{-3} \text{ s}^{-1} \quad (30)$$

$$R_{H_2O} = -rsr - rws \ ; \ \text{in mol m}^{-3}\text{s}^{-1} \quad (31)$$

$$R_{H_2} = 3rsr + rws \ ; \ \text{in mol m}^{-3}\text{s}^{-1} \quad (32)$$

$$R_{CO} = rsr - rws \ ; \ \text{in mol m}^{-3}\text{s}^{-1} \quad (33)$$

$$R_{CO_2} = rws \ ; \ \text{in mol m}^{-3}\text{s}^{-1} \quad (34)$$

Chapter 3

3. Methodology

3.1. Introduction

Chapter 2 introduced the reactor model equations that were used used in this investigation. These equations were implemented in a commercial simulation package, COMSOL Multiphysics, which uses the finite element method (FEM) to solve partial differential equations.

COMSOL Multiphysics has a large number of built-in modules that represent different types of physical behaviors. For this study, four modules are used:

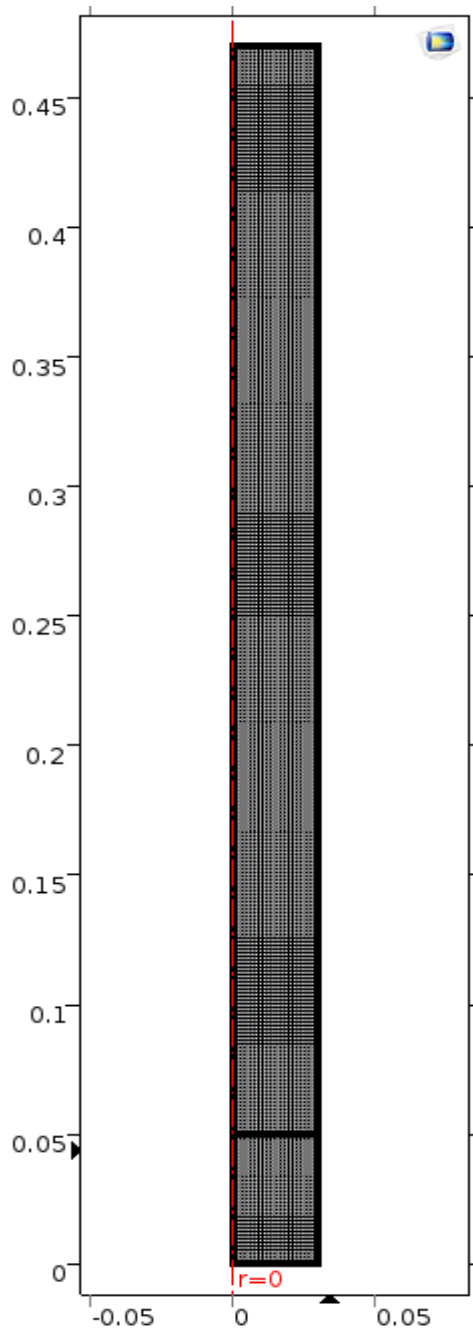
- Non-Isothermal Flow
- Heat Transfer in Solids
- Transport of Concentrated Species
- Convection-Diffusion Equation

The Non-Isothermal flow module was used to calculate the flow pattern, the energy balance of the fluid and the pressure drop. The Heat Transfer in Solids module was used to calculate the energy balance in the solid phase. The Transport of Concentrated Species was used to calculate the mass balance in the fluid with a base on mass fractions, which would be a difference with the equations found in literature and showed in Section 2.2.4 which are based on mole fractions. The Convection-Diffusion Equation was used to calculate the mass balance for the solid by setting all of the differential terms and the velocity equal to zero. The equation ends up to be the source term f only. Thus, this source term is replaced by the equation that represents the mole balance for the solid, which is not a differential equation. The exact form of the equations and their implementation in COMSOL is discussed in the following sections.

Geometry

The geometry is shown in figure 4. The extended inlet can be seen in b).

a)



b)

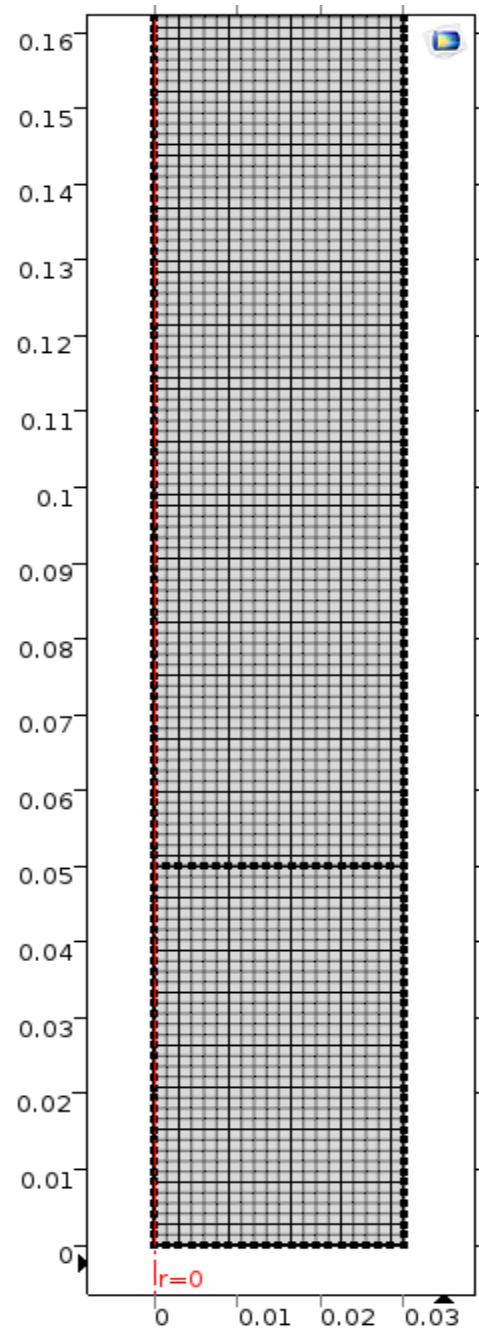


Figure 4: Geometry of the modeled reactor in a) and b) is a zoom-in of the geometry to visualize the mesh style.

The image in the left hand side is the complete geometry of the model which counts with two rectangles. The lower rectangle is just an extended inlet that helps to improve the convergence of the numerical model and therefore no reaction happens in this part of the reactor and it only represents a tube without catalyst particles. The upper rectangle represents the packed bed, here is where the catalyst particles are represented as a porous medium and the reaction happens. The model is axisymmetric and the symmetry boundary condition is placed at the left side of the geometry, which leaves the wall at the right hand side of the geometry.

$$\frac{\partial \omega_{i,fluid}}{\partial r} = \frac{\partial T_{fluid}}{\partial r} = \frac{\partial T_{Solid}}{\partial r} = 0 \quad \text{at } r = 0 \quad (35)$$

The total dimensions of the geometry are 0.03 meters wide (reactor radius) and 0.47 meters high. The extension of the inlet has 0.05 meters high leaving a packed bed of 0.42 meters long. The flow moves from the base of the geometry up to the upper part where the outlet is placed.

$$\frac{\partial \omega_{i,fluid}}{\partial z} = \frac{\partial T_{fluid}}{\partial z} = \frac{\partial T_{Solid}}{\partial z} = 0 \quad \text{at } z = L \quad (36)$$

The catalyst pellets are taken into account mathematically on the equations and they are modeled to have a diameter of 0.006 m.

An orthogonal structured mesh is selected to be used on the model because of its simplicity, because the geometry does not have any complexity and because when grid lines are approximately aligned with the flow artificial diffusion can be minimized¹.

3.1.1. Non-isothermal flow

$$\rho(u \cdot \nabla)u = \nabla \cdot \left[-pI + \mu(\nabla u + (\nabla u)^T) - \frac{2}{3}\mu(\nabla \cdot u)I \right] + F \quad (5)$$

$$\nabla \cdot (\rho u) = 0 \quad (6)$$

The model is developed using volume averaged Navier-Stokes equation using an inlet velocity of $v_o = 0.3 \text{ m/s}$ and using the boundary condition “Pressure, no viscous stress” at the outlet and a slip condition at the wall. The slip condition is more physical than the no slip condition for the

¹ taken from professor Carlos Lange's MECE 539 lecture notes

case of this model, because the force that affects the flow distribution is related to the body force, which depends on the permeability which is modeled as a function of the radial position. However, the no slip condition reflects the loss of momentum from the fluid to the wall which in this case is not physical as it was already accounted for.

The problem is calculated for a pressure of 25 bar.

Ergun equation is used to obtain the permeability and volume forces are used to take into account for the porous medium.

For r-direction

$$Volume\ force = -\frac{u}{D_p} \cdot \left(\frac{1-\phi}{\phi^3}\right) \left[150 \frac{\mu(1-\phi)}{D_p} + 1.75\rho u\right] N/m^3 \quad (37)$$

With u as the r-direction velocity.

For z-direction

$$Volume\ force = -\frac{w}{D_p} \cdot \left(\frac{1-\phi}{\phi^3}\right) \left[150 \frac{\mu(1-\phi)}{D_p} + 1.75\rho w\right] N/m^3 \quad (38)$$

With w as the z-direction velocity, D_p as the particle diameter equal to 0.006[m], μ as the dynamic viscosity, ϕ as the porosity and ρ as the density of the fluid calculated automatically by the software assuming an ideal gas condition at a pressure of 25 [bar].

There are two main models that are compared in this thesis. One with a constant porosity of 0.38 and other one with a variable porosity that depends on the radius position. This last one in average is also 0.38. The porosity is discussed further into this thesis.

The dynamic viscosity is calculated for each component of the reaction using experimental isobaric data at 25[bar] taken from a NIST² Chemistry WebBook tool called “Thermophysical Properties of Fluid Systems”. The data is obtained temperature dependent and an equation is created for each dynamic viscosity.

² National Institute of Standards and Technology website: <http://webbook.nist.gov/chemistry/fluid/>

$$\mu_{CH_4} = 2.498 \times 10^{-8} \times T + 4.631 \times 10^{-6} \quad (39)$$

$$\mu_{H_2O} = -6.575 \times 10^{-12} \times T^2 + 5.171 \times 10^{-8} \times T - 7.433 \times 10^{-6} \quad (40)$$

$$\mu_{H_2} = -2.725 \times 10^{-12} \times T^2 + 1.919 \times 10^{-8} \times T + 3.849 \times 10^{-6} \quad (41)$$

$$\mu_{CO} = 3.818 \times 10^{-8} \times T + 6.898 \times 10^{-6} \quad (42)$$

$$\mu_{CO_2} = -9.673 \times 10^{-12} \times T^2 + 4.825 \times 10^{-8} \times T + 2.759 \times 10^{-6} \quad (43)$$

Having all of the viscosities the equation of Hering and Zipperer can be used to obtain the dynamic viscosity of the mixture

$$\mu_f = \frac{\sum(y_i \mu_i \sqrt{M_i})}{\sum(y_i \sqrt{M_i})} \quad (44)$$

With y_i as the mole fraction of the i -th component and M_i as its molar weight.

3.1.2. Mass balance for fluid

The mass balance for the fluid is represented by the COMSOL module called Transport of concentrated species which uses the equations:

$$\nabla \cdot (-\rho D_e \nabla \omega_{i,fluid}) + \rho(u \cdot \nabla) \omega_{i,fluid} = -k_m \cdot a_m \cdot \rho_{fluid} \cdot (\omega_{i,fluid} - \omega_{i,solid}) \quad (45)$$

$$\frac{\partial \omega_{i,fluid}}{\partial r} = 0 \quad \text{at } r = R \quad (46)$$

To use this module is necessary to set up some parameters. The diffusion coefficient for every component is one of them. In the heterogeneous model selected to use in this work there is no diffusion coefficient for the bed, instead a dispersion coefficient equal for every component is used (which has the same units of the diffusion coefficient) for the axial and radial directions.

The dispersion coefficients were calculated using the following equations

$$(Pe_m)_r = \frac{D_B v_s}{D_{er}} \quad (47)$$

$$(Pe_m)_z = \frac{D_B v_s}{D_{ea}} \quad (48)$$

$$(Pe_m)_r = 10 \quad (49)$$

$$(Pe_m)_z = 2 \quad (50)$$

$$D_B = \frac{D_T}{\frac{3}{2}(D_T/D_P)(1 - \phi) + 1} \quad (51)$$

With D_{er} as the radial dispersion coefficient, D_{ea} as the axial dispersion coefficient, $(Pe_m)_r$ as the radial Peclet number for mass transfer, $(Pe_m)_a$ as the axial Peclet number for mass transfer, D_B as the hydraulic diameter, D_T as the tube diameter and D_P as the particle diameter.

The inflow is set on mole fractions

$$y_{CH_4} = 0.25 \quad at \ z = 0 \quad (51)$$

$$y_{H_2O} = 0.75 \quad at \ z = 0 \quad (52)$$

With CO_2 calculated by the software as a mass constraint and a mole fraction equal to zero for the rest of the components.

The reactions are calculated in $kg/(m^3 \cdot s)$ as:

For CH_4

$$-k_m \cdot a_m \cdot \rho_{fluid} \cdot (\omega_{CH_4,fluid} - \omega_{CH_4,solid}) \quad (53)$$

For H_2O

$$-k_m \cdot a_m \cdot \rho_{fluid} \cdot (\omega_{H_2O,fluid} - \omega_{H_2O,solid}) \quad (54)$$

For H_2

$$-k_m \cdot a_m \cdot \rho_{fluid} \cdot (\omega_{H_2,fluid} - \omega_{H_2,solid}) \quad (55)$$

For CO

$$-k_m \cdot a_m \cdot \rho_{fluid} \cdot (\omega_{CO,fluid} - \omega_{CO,solid}) \quad (56)$$

For CO₂

$$-k_m \cdot a_m \cdot \rho_{fluid} \cdot (\omega_{CO_2,fluid} - \omega_{CO_2,solid}) \quad (57)$$

With $a_m = \frac{\Delta S}{\Delta V} = \frac{S}{V}$ as particle surface area per unit bed volume, k_m as the mass transfer coefficient, $\omega_{i,fluid}$ as the mass fraction for a component on the fluid and $\omega_{i,solid}$ as the mass fraction for a component in the solid (or catalyst particle)

$$k_m = \frac{Sh * D}{D_p} \quad (58)$$

$$Sh = 2 + 1.1 * Sc^{1/3} * Re_b^{0.6} \quad (59)$$

$$Sc = \frac{\mu_f}{\rho * D} \quad (60)$$

$$Re_b = \frac{\rho v_s D_p}{\mu_f} \quad (61)$$

With Sh as the Sherwood number, Sc as the Schmidt number, D as the molecular diffusion of the system and Re_b as the Reynolds number of the bed.

$$D = \sum_{i=1}^n \frac{D_{im}}{n} \quad (62)$$

$$D_{im} = \left(\sum_{\substack{j=1 \\ j \neq i}}^n \frac{y_j}{D_{ij}} \right)^{-1} \quad (63)$$

$$D_{ij} = \frac{1.013 \times 10^{-2} T^{1.75} [1/M_i + 1/M_j]^{0.5}}{P \left[(\Sigma v)_i^{1/3} + (\Sigma v)_j^{1/3} \right]^2} \quad (64)$$

With D_{im} as molecular diffusion in m/s of the i -th component, D_{ij} as the binary molecular diffusion, P as absolute pressure in Pascal, T as temperature in Kelvin and Σv_i as the diffusion volume of a molecule. The density is calculated automatically by the software using the molar weights of the components and assuming an ideal gas condition at 25 [bar] of pressure.

$$M_{CH_4} = 16.04 \quad (65)$$

$$M_{H_2O} = 18.02 \quad (66)$$

$$M_{H_2} = 2.02 \quad (67)$$

$$M_{CO} = 28.01 \quad (68)$$

$$M_{CO_2} = 44.01 \quad (69)$$

$$(\Sigma v)_{CH_4} = 24.42 \quad (70)$$

$$(\Sigma v)_{H_2O} = 12.7 \quad (71)$$

$$(\Sigma v)_{H_2} = 7.07 \quad (72)$$

$$(\Sigma v)_{CO} = 18.9 \quad (73)$$

$$(\Sigma v)_{CO_2} = 26.9 \quad (74)$$

3.1.3. Mass balance for the solid

To implement the solid mass balance equation on Comsol, the Convection-diffusion equation module is used. All of its parameters are set as zero with the exception of the source term which is set as

$$k_m a_m \rho_{fluid} (\omega_{CH_4, fluid} - \omega_{CH_4, solid}) - \eta (1 - \phi) \left(- (R_{CH_4}) \right) M_{CH_4} = 0 \quad (75)$$

$$k_m a_m \rho_{fluid} (\omega_{H_2O,fluid} - \omega_{H_2O,solid}) - \eta(1 - \phi) \left(-(R_{H_2O}) \right) M_{H_2O} = 0 \quad (76)$$

$$k_m a_m \rho_{fluid} (\omega_{H_2,fluid} - \omega_{H_2,solid}) - \eta(1 - \phi) \left(-(R_{H_2}) \right) M_{H_2} = 0 \quad (77)$$

$$k_m a_m \rho_{fluid} (\omega_{CO,fluid} - \omega_{CO,solid}) - \eta(1 - \phi) \left(-(R_{CO}) \right) M_{CO} = 0 \quad (78)$$

$$k_m a_m \rho_{fluid} (\omega_{CO_2,fluid} - \omega_{CO_2,solid}) - \eta(1 - \phi) \left(-(R_{CO_2}) \right) M_{CO_2} = 0 \quad (79)$$

3.1.4. Energy balance for fluid

The energy balance for the fluid is represented by the Non-isothermal flow model with the equation:

$$\rho C_p u \cdot \nabla T = \nabla \cdot (k \nabla T) + Q \quad (80)$$

Using the source term Q as:

$$-h_{fs} a_m (T_f - T_s) \quad (81)$$

With h_{fs} as the fluid-solid heat transfer coefficient, T_f as the temperature of the fluid and T_s as the temperature of the solid particles.

The radial and axial thermal conductivity coefficients (k_{rf} and k_{af}) can be obtained by using the following equations

$$(\text{Pe}_H)_{rf} = \frac{GC_p D_P}{k_{rf}} \quad (82)$$

$$(\text{Pe}_H)_{af} = \frac{GC_p D_P}{k_{af}} \quad (83)$$

$$\frac{1}{(\text{Pe}_H)_{rf}} = 0.1 + \frac{0.66\phi}{\text{Re}_b \text{Pr}} \quad (84)$$

$$\frac{1}{(\text{Pe}_H)_{af}} = \frac{0.73\phi}{\text{Re}_b \text{Pr}} + \frac{0.5}{(1 + (9.7\phi/\text{Re}_b \text{Pr}))} \quad (85)$$

With $(Pe_H)_{rf}$ as the radial Peclet number for heat transfer, $(Pe_H)_{af}$ as the axial Peclet number for heat transfer, Pr as the Prandtl number, G as the superficial mass velocity defined as ρv_s and C_P as the heat capacity at constant pressure is calculated using the following formula

$$C_{P_f} = \omega_{CH_4} C_{P_{CH_4}} + \omega_{H_2O} C_{P_{H_2O}} + \omega_{H_2} C_{P_{H_2}} + \omega_{CO} C_{P_{CO}} + \omega_{CO_2} C_{P_{CO_2}} \quad (86)$$

$$C_{P_{CH_4}} = 5.657 \times 10^{-2} \times T + 1.893 \times 10 \quad (87)$$

$$C_{P_{H_2O}} = 6.224 \times 10^{-11} \times T^4 - 2.677 \times 10^{-7} \times T^3 + 4.336 \times 10^{-4} \times T^2 - 3.024 \times 10^{-1} \times T + 1.162 \times 10^2 \quad (88)$$

$$C_{P_{H_2}} = 3.088 \times 10^{-6} \times T^2 - 2.739 \times 10^{-3} \times T + 2.988 \times 10 \quad (89)$$

$$C_{P_{CO}} = 3.437 \times 10^{-3} \times T + 2.845 \times 10 \quad (90)$$

$$C_{P_{CO_2}} = -1.089 \times 10^{-5} \times T^2 + 3.318 \times 10^{-2} \times T + 3.227 \times 10 \quad (91)$$

With the individual heat capacity equations created from experimental data at 25[bar] obtained from the same NIST WebBook as the dynamic viscosities mentioned in 3.3.2.

$$h_{fs} = \frac{Nu * k_f}{D_p} \quad (92)$$

$$Nu = 2 + 1.1Pr^{1/3}Re_b^{0.6} \quad (93)$$

$$Pr = \frac{C_P \mu}{k_f} \quad (94)$$

With k_f as the thermal conductivity of the fluid, calculated using Wilke's approach (Wilke, 1950)

$$k_f = k_{mix} = \sum_{i=1}^n \frac{x_i k_i}{\sum_{j=1}^n x_j \Phi_{ij}} \text{ in } \frac{W}{mK} \quad (95)$$

$$\Phi_{ij} = \frac{\left[1 + \left(\frac{\mu_i}{\mu_j} \right)^{0.5} \left(\frac{M_j}{M_i} \right)^{0.25} \right]^2}{\sqrt{8} [1 + (M_i/M_j)]^{0.5}} \quad (96)$$

$$\Phi_{ii} = 1 \quad (97)$$

$$k_{CH_4} = 1.947 \times 10^{-4} \times T - 2.744 \times 10^{-2} \quad (98)$$

$$k_{H_2O} = 2.603 \times 10^{-8} \times T^2 + 8.420 \times 10^{-5} \times T - 1.188 \times 10^{-2} \quad (99)$$

$$k_{H_2} = 4.943 \times 10^{-4} \times T + 3.080 \times 10^{-2} \quad (100)$$

$$k_{CO} = 6.210 \times 10^{-5} \times T + 8.545 \times 10^{-3} \quad (101)$$

$$k_{CO_2} = -1.523 \times 10^{-8} \times T^2 + 9.631 \times 10^{-5} \times T - 1.018 \times 10^{-2} \quad (102)$$

With the individual thermal conductivity equations created from experimental data at 25 bar obtained from the same NIST WebBook as the dynamic viscosities mentioned in 3.3.2.

On addition to that, a heat flux is imposed as a boundary condition to the walls of the reactor:

$$-k_{rf} \frac{\partial T_f}{\partial r} = U_f (T_f - T_{ext}) \quad \text{at } r = R \quad (103)$$

With $T_{ext} = 1123[K]$ and U_f as the overall heat transfer coefficient of the fluid.

$$\frac{1}{U_f} = \frac{1}{h_{wf}} + \left(\frac{D_T}{2k_W} \right) \ln \left(\frac{D_o}{D_T} \right) + \frac{D_T}{D_o} \frac{1}{h_o} \quad (104)$$

With h_o as the external heat transfer coefficient, k_W as the thermal conductivity of the wall (in this case assumed to be copper), D_o as the external diameter of the reactor and h_{wf} as the wall-fluid heat transfer coefficient.

$$h_o = 1000 \text{ W}/(\text{m}^2 \cdot \text{K}) ; k_W = 20 \text{ W}/(\text{m} \cdot \text{K}) ; D_o = 0.062 \text{ m}$$

$$h_{wf} = \frac{0.2 \text{Pr}^{1/3} \text{Re}_b^{0.8} k_f}{D_p} \quad (105)$$

3.1.5. Energy balance for solid

The solid mole balance is represented by the Comsol module Heat transfer in solids

$$0 = \nabla \cdot (k \nabla T_s) + Q \quad (106)$$

$$\frac{\partial T_s}{\partial z} = 0 \quad \text{at } z = 0 \quad (107)$$

Using the heat source term Q to input three different sources. The first one is the interaction of the fluid with the solid

$$h_{fs} a_m (T_f - T_s) \quad (108)$$

The second one is the heat resulting from the endothermic reforming reaction taking place in the solid

$$\eta (R_{CH_4}) (1 - \phi) \Delta H_R \quad ; \quad \Delta H_R = 206200 \text{ J/mol} \quad (109)$$

And the last one is the heat resulting from the slightly exothermic water-gas shift reaction taking place in the solid

$$\eta (-R_{CO_2}) (1 - \phi) \Delta H_{R2} \quad ; \quad \Delta H_{R2} = -41000 \text{ J/mol} \quad (110)$$

The radial and axial thermal conductivity of the solid are obtained by using the equations:

$$k_{rs} = k_{as} = \frac{2k_f(1-\phi)^{0.5}}{(1-(k_f B/k_p))} \left[\frac{(1-(k_f/k_p))B}{(1-(k_f B/k_p))^2} \ln\left(\frac{k_p}{Bk_f}\right) - \frac{B+1}{2} - \frac{B-1}{(1-(k_f B/k_p))} \right] \quad (111)$$

$$B = C \left(\frac{1-\phi}{\phi} \right)^{10/9} \quad (112)$$

C equal to 1.25 for spheres

$k_p = 9.5 \text{ W/mK}$ Thermal conductivity of alumina at 1000 K

And by setting the properties of the solid of the following way:

$$\rho = (1 - \phi) \cdot \rho_{solid} \quad (113)$$

$$\rho_{solid} = 1600 \text{ kg/m}^3 \quad (114)$$

$$C_p = 1205 \text{ J}/(\text{kg} \cdot \text{K}) \quad \text{At } 1000 \text{ K} \quad (115)$$

Additionally, a heat flux is imposed as a boundary condition to the walls of the reactor:

$$-k_{rs} \frac{\partial T_s}{\partial r} = U_s(T_s - T_{ext}) \quad \text{at } r = R \quad (116)$$

With $T_{ext} = 1123 \text{ K}$ and U_s as the overall heat transfer coefficient of the solid.

$$\frac{1}{U_s} = \frac{1}{h_{ws}} + \left(\frac{D_T}{2k_W} \right) \ln \left(\frac{D_o}{D_T} \right) + \frac{D_T}{D_o} \frac{1}{h_o} \quad (117)$$

With h_o as the external heat transfer coefficient, k_W as the thermal conductivity of the wall (in this case assumed to be copper), D_o as the external diameter of the reactor and h_{ws} as the wall-solid heat transfer coefficient.

$$h_o = 1000 \text{ W}/(\text{m}^2 \cdot \text{K}) ; k_W = 20 \text{ W}/(\text{m} \cdot \text{K}) ; D_o = 0.062 \text{ m}$$

$$h_{ws} = \frac{2.12k_{rs}}{D_p} \quad (118)$$

3.1.6. Radial porosity variation

Literature shows that in average, the radial porosity on a packed bed reactor varies. Because of this, an important step in this research was to develop an individual equation that could follow those patterns. An equation which could emulate what was found in the experimental studies of Bay et al. (1997) and in the data obtained by the modeling studies of Zeiser et al. (2001).

After obtaining an equation that more or less followed the behavior shown in the literature data, the equation was tuned up using both, the Bay et al. and the Zeiser et al. data, using a non-linear solver with the following equation and parameters

Form of the equation:

$$\phi = a * \exp(b * D_w) * \cos(c * D_w + d) + e + f * g^{-D_w} \quad (117)$$

With D_w as the dimensionless distance from the wall

$$D_w = \frac{R_t - r}{R_p} \quad (118)$$

With ϕ as the porosity in each point of the radius, R_t as the tube radius, R_p as the particle radius and r as the radius in each point. For each of those points, a squared error (difference powered to two) was calculated and summed through the whole radius. This sum of squared errors is done for the data of Zasier (2001) and Bay (1997) obtaining two final errors for each one of them. They are going to be called E1 and E2 respectively. Knowing this, the restrictions for the solver are the following.

Changing a, b, c, d, e, f and g:

$$\text{Minimize } E1 + E2 \quad (119)$$

$$E1 - E2 = 0 \quad (120)$$

$$\phi_{wall} = 0.99 \quad (121)$$

$$\phi_{average} = 0.38 \quad (122)$$

This path of tuning the proposed equation aims to obtain an equation in the middle of the other two. Thus, the same sum of squared errors can be obtained for E1 and E2 and in this case its value is of 0.16.

It is easy to see in Figure 5 that the new equation obtained for the radial porosity achieves the goal and it is located between the other two curves found in literature. Accordingly, it delivers enough confidence, and this variable porosity equation is the one used on every porosity term of the final model.

The following new equation obtained is the one used to simulate the variable porosity that is developed in a packed bed reactor model

$$\phi = 0.2128 * \exp(-0.155D_w) * \cos(3.5D_w - 0.6146) + 0.367 + 0.449 * 296.17^{-D_w} \quad (123)$$

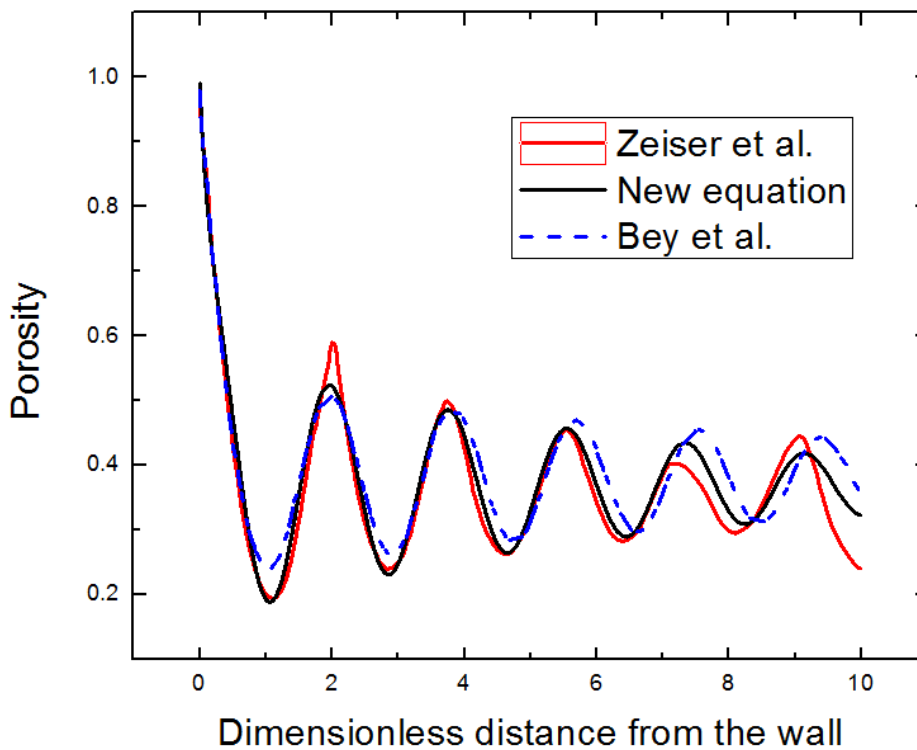


Figure 5: Developed equation of radial porosity distribution compared against the results obtained by Zeiser et al. (2001) and Bay et al. (1997).

3.1.7. Procedure in brief

After setting up all of the aforementioned parameters and boundary conditions on the selected modules of the software, a first approach to the model was to run it using the kinetics obtained from Haberman and Young (2004). The rates for each component were used as shown in the Section 2.3.3.3 and the effectiveness factor was taken as one.

The next step on the procedure, is to create a one dimensional diffusion model with chemical reactions of one of the spherical catalyst pellets. With this kind of model, and using the same kinetics, one can calculate the reaction rates with the correct effectiveness factors. This because in the reactor, all of the chemical reactions finally take place within the pellets. Thus, one simulation of this model makes us obtain accurate rate data under chosen conditions.

If this is done many times, over a determined range of possible conditions, all these reaction rate data computed can be stored in the form of a look-up table. This look-up table with all of the precomputed rates and effectiveness factors can be coupled with the reactor model later on, to give form to the final model. This is the procedure followed. The look-up tables are explained in Section 3.1.9.

3.1.8. Computing the effectiveness factor

As already mentioned, a new model which represents one of the pellets is needed on order to be able to compute the effectiveness factor of the reaction. As known, the effectiveness factor is the average reaction rate for a catalyst pellet divided by the reaction rate evaluated at surface conditions. This model uses purely diffusion and represents how the species move and react within the pellet. The model is one dimensional and axisymmetric and later on is the model used to create the look-up tables.

In accordance with the reactor model, the one dimensional model has a length of 0.003[m] which corresponds to the radius on one of the particles of the reactor. Because it is a symmetrical model, that condition is on charge of accounting for the missing length to obtain the full diameter of the particle. In fact, the software does more than that, it can rotate the linear model over the symmetry line and show the results on a full circle area in two dimensions, the same way that it can rotate the two dimensional reactor model to show the results in a three dimensional cylinder.

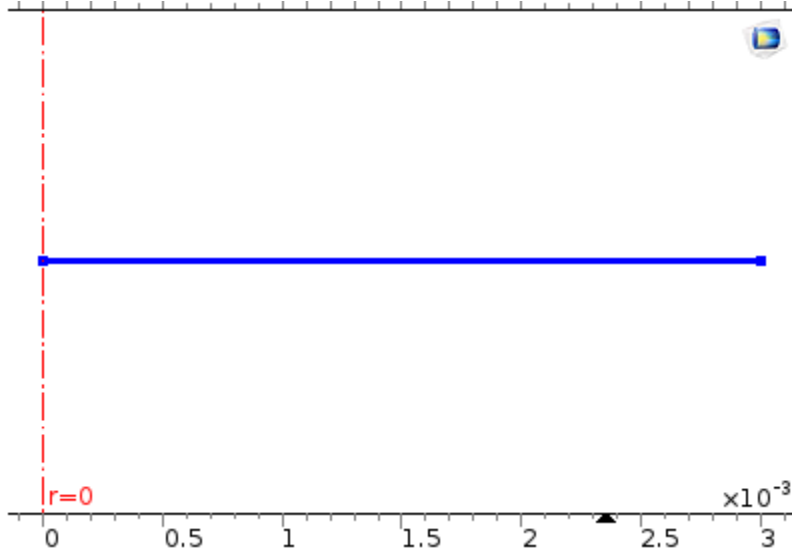


Figure 6: Geometry of one dimensional diffusion model

The model is developed over the transport of concentrated species module in COMSOL and it is set to account exclusively for diffusion (Fick's law). Figure 6 is the geometry of the model and it represents one pore of the pellet. The following are the governing equations.

$$\nabla \cdot \left(-\rho D_i \nabla \omega_i - \rho \omega_i D_i \frac{\nabla M_n}{M_n} \right) = R_i \quad (124)$$

$$M_n = \left(\sum_i \frac{\omega_i}{M_i} \right)^{-1} \quad (125)$$

In this case an effective diffusion is used due to the nature of the problem

$$D_{eff,i} = \frac{\varepsilon D_{pore,i}}{\tau} \quad (126)$$

With ε as the porosity of the particle which in this case is assumed to be 0.4, τ as the tortuosity assumed in this case to be 2 and $D_{pore,i}$ as the pore diffusion coefficient of the component i.

$$\frac{1}{D_{pore,i}} = \frac{1}{D_{im}} + \frac{1}{D_{iK}} \quad (127)$$

The molecular diffusion is calculated in the same manner, with the same parameters and temperature dependent equations for each component as calculated for the packed bed reactor model. The same happens with the density, calculated assuming ideal gas and a pressure of 25[bar].

$$D_{im} = \left(\sum_{\substack{j=1 \\ j \neq i}}^n \frac{y_j}{D_{ij}} \right)^{-1} \quad (128)$$

$$D_{ij} = \frac{1.013 \times 10^{-2} T^{1.75} [1/M_i + 1/M_j]^{0.5}}{P \left[(\Sigma \nu)_i^{1/3} + (\Sigma \nu)_j^{1/3} \right]^2} \quad (129)$$

The Knudsen diffusion coefficient $D_{K,i}$ is also needed to calculate the pore diffusion coefficient

$$D_{K,i} = 48.5 d_p \left(\frac{T}{M_i} \right)^{\frac{1}{2}} \quad (130)$$

With d_p as the pore diameter in this case assumed to be 10[nm] and M_i as the molar weight of the component i.

The model is isobaric and isothermal with a pressure of 25[bar] and a temperature that has to be set depending on the study. As an example let's say that the temperature is 1123[K].

The mass fractions at the end of the interval that would correspond to the surface of the sphere can also be set differently depending on the study. For the example they are set as

$$\omega_{CH_4} = 0.23 \quad (131)$$

$$\omega_{H_2O} = 0.77 \quad (132)$$

And the rest are set to zero.

The reactions use the global kinetics described by Haberman and Young (2004) which makes the source term:

$$R_{CH_4} = -rsr \times M_{CH_4} \quad (133)$$

$$R_{H_2O} = (-rsr - rws) \times M_{H_2O} \quad (134)$$

$$R_{H_2} = (3rsr + rws) \times M_{H_2} \quad (135)$$

$$R_{CO} = (rsr - rws) \times M_{CO} \quad (136)$$

$$R_{CO_2} = rws \times M_{CO_2} \quad (137)$$

The rates are multiplied by the molar weights of its corresponding specie to obtain the units of $kg/(m^3s)$. The rate R_{H_2O} actually is not input in the model because ω_{H_2O} is calculated by the software as from mass constraint.

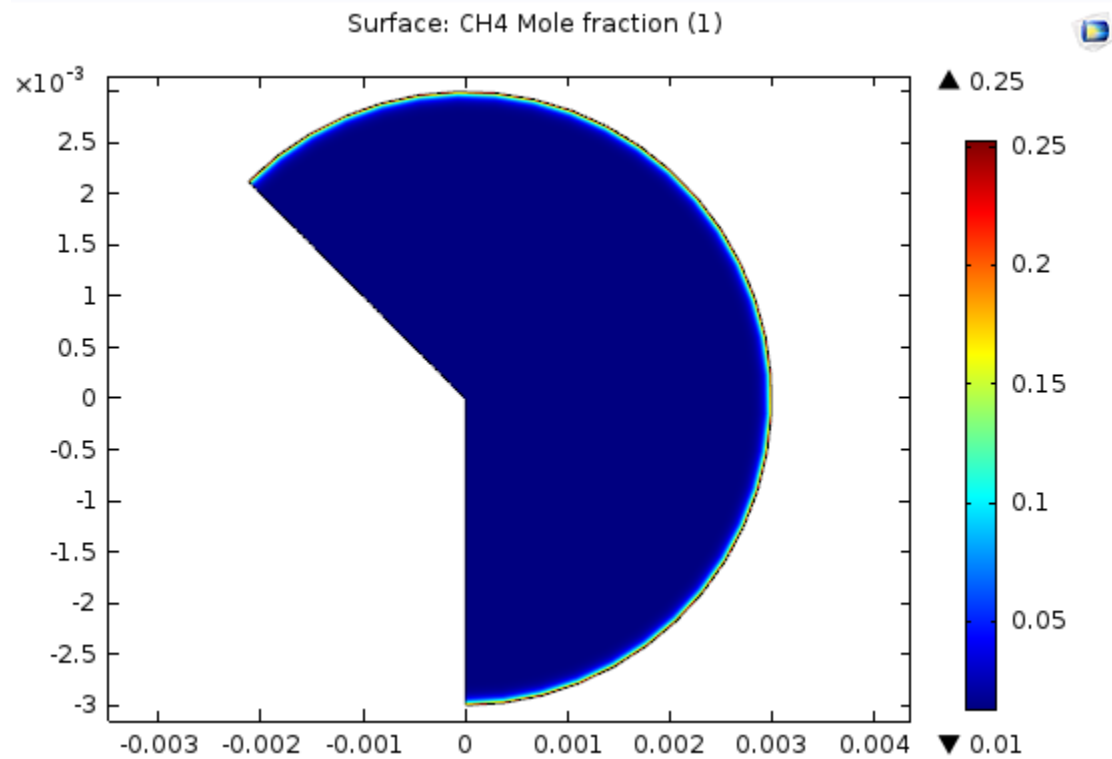


Figure 7: Methane mole fraction, diffusion model

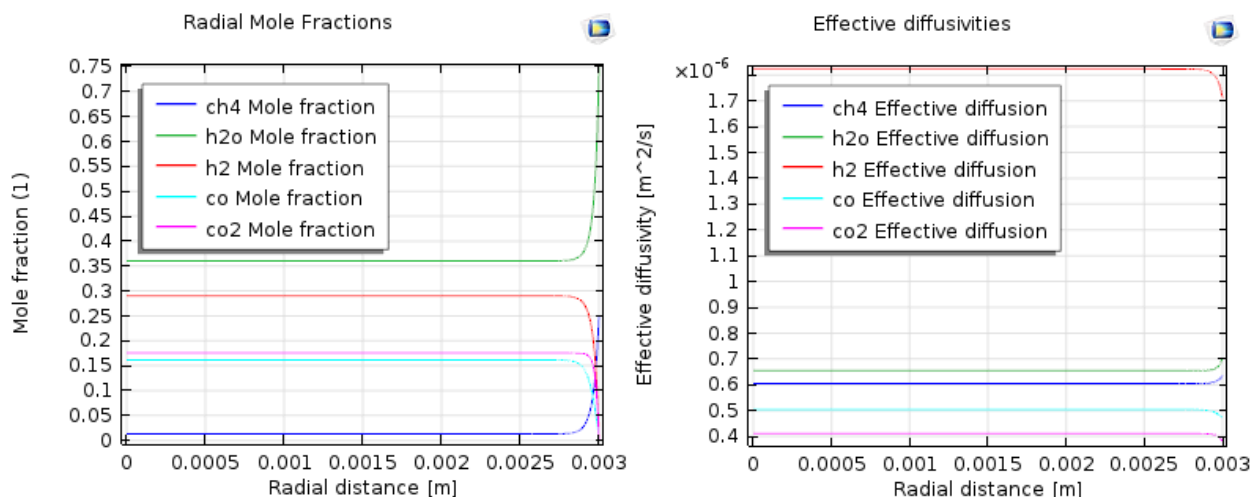


Figure 8: Mole fractions (Left) and effective diffusivities (Right), diffusion model

The reason why the reaction happens in the neighborhood of the surface of the particle is that, as shown in the figure above, the effective diffusivities are very small (around the order of 10^{-6}). The mass fraction for methane can be seen in Figure 7 and for every component mass fractions and effective diffusivities it is shown in Figure 8.

This example shows how the diffusion model works and it is a realistic example because the evaluated conditions are the ones found at the inlet of the reactor, at the moment when the molecules enter to the pores of the catalyst.

This is a very important model for this work because this model is the one used to build the look-up tables that are applied in the final model developed. It would be very expensive, computationally speaking, to calculate a complete second model with all of its equations and parameters for each point of the reactor, to obtain the real kinetics for each of those points. The computing times would increase enormously. This is the main reason why the look-up tables are needed for this study.

3.1.9. Look-up tables and errors

In this work we call look-up table to a group of pre-computed reaction rates already multiplied for its correspondent effectiveness factor (just called “rate data” for simplicity in this section), stored in an efficient manner. This rate data is calculated over a range of possible combinations of

conditions. These reaction conditions are temperature and mole fractions of all the components of the reaction. Each of them is a dimension for the look-up table. The look-up table used in this work has six dimensions. One for temperature and one more for each specie. This technique is found in literature and it is called sometimes repro-modeling (Meisel & Collins, 1973; T. Turányi, 1994; Tamás Turányi, 1994) and most recently in the work of Votsmeier (Votsmeier, 2009). To build the tables, first, one has to identify the important parameters which in this case are methane, water, hydrogen, carbon monoxide and carbon dioxide, with temperature as the last parameter. Then a range is set for each parameter. If the parameters range is broad the table becomes more broadly useful but it also becomes more computationally expensive to build and to access. Therefore, it is very important to select ranges that suit the necessities of the model. Secondly, it is important to determine the resolution or grid of the table. In literature, the procedure is to gradually increase the size of the grid, increasing it only in one of the dimensions at each step (Nien, Mmbaga, Hayes, & Votsmeier, 2013). To start, the table contains two values (nodes) for each dimension, corresponding to the ending points of the ranges, the table is usually denoted with one number per dimension. This number, is the number of nodes of the corresponding grid. For this case the starting table would be denoted [2 2 2 2 2 2]. When a value between two nodes is required, the look-up table uses an interpolation function, called spline, to calculate it. When a dimension grid is increased, one node is placed between two already existing nodes. This means that a dimension would increase from 2 to 3, then to 5, then to 9 and so on. Additionally, at each step a prediction error must be computed. For example, after building table [2 2 2 2 2 2], tables [3 2 2 2 2 2], [2 3 2 2 2 2], [2 2 3 2 2 2], [2 2 2 3 2 2], [2 2 2 2 3 2], [2 2 2 2 2 3] are built; the one with the lowest error will be accepted and will become the new starting point. This process goes on until an acceptable error is achieved. To calculate the error a data test of 10,000 combinations of the 6 parameters is used. The formula used to calculate the error is

$$error = \left[\sum_{i=1}^N \frac{1}{N} \left(\frac{R_i - R_{spline,i}}{r} \right)^2 \right]^{0.5} \quad (138)$$

For this work, the tables were built by A. Fadic following the procedures shown by Votsmeier (Votsmeier, 2008) and Nien (Nien et al., 2013).

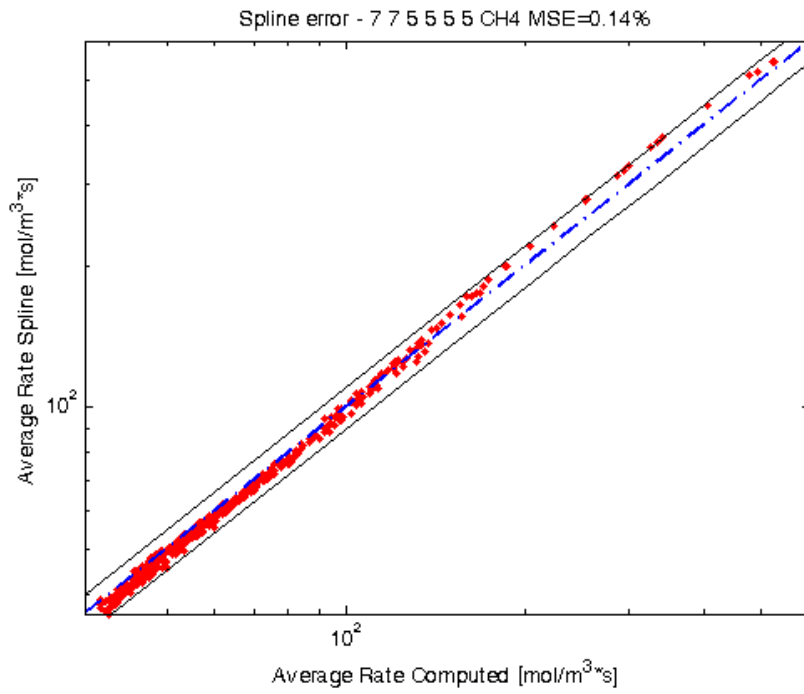


Figure 9: Spline function rate errors for methane

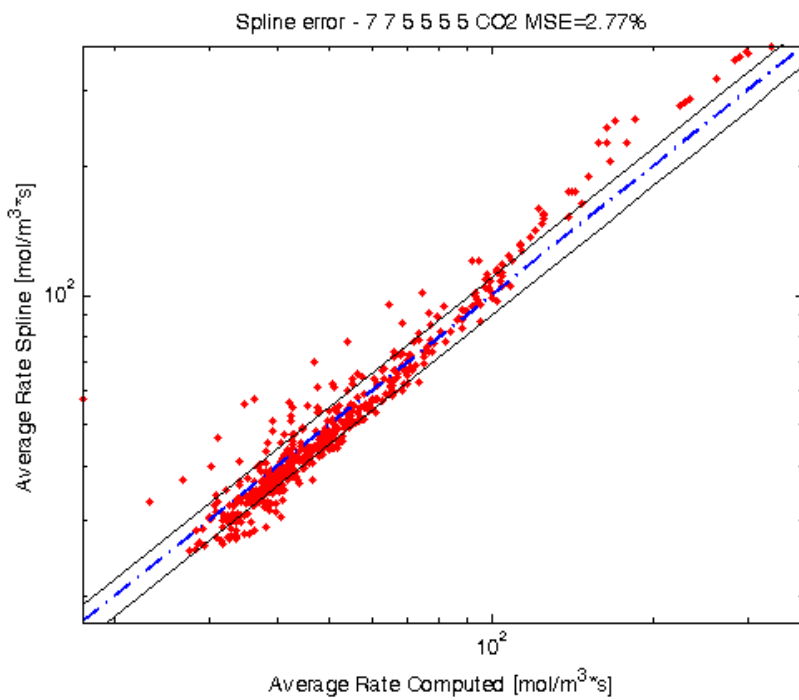


Figure 10: Spline function rate errors for carbon dioxide

Finally, a chosen density of grid points is accepted for each dimension. The errors of this procedure can be easily obtained and are shown in the following Figure 9 and Figure 10 for CH₄ and CO₂ respectively.

The errors arise because of the grid density, the higher the density the smaller the error. However, having a higher the density makes the look-up table more computationally expensive to create and to access. From here the importance to increase the grid gradually and only until a point where the error is acceptable, with reasonable computation times and not further. This explain the error in the tables. The errors are calculated by comparing random data points. These random points are calculated two times. The first time, calculated using the only the diffusion model, the second time, calculated only using the look-up table. Then, the error between the two values can be calculated for each random data pint. It is worth to mention that the table has a real value on each node of the grid for each corresponding dimension, and when a value between two nodes is required, the table interpolates using the spline function.

The final accepted look-up table, then is coupled with the COMSOL reactor model developed previously. However, now the model will use kinetics with a specific effectiveness factor for each point of the reactor which will be obtained from the tables. The model will input to the look-up tables the temperature of the solid, and the mole fraction in the solid of each of the five species of the reaction. This will be done for each point of the reactor. In exchange, the look-up table will give to the model a rate of production (with its corresponding effectiveness factor) for each component as an output for each of those points.

Chapter 4

4. Results and discussion

In this chapter, the results of the final packed bed reactor model, which uses the rate data from the look-up tables, are shown. Additionally, a sensitivity analysis to measure how the model parameters affect the overall model and a study to determine the importance of the porosity variation is carried out. Other cases of changes in some boundary conditions and their effects are also studied. However, before obtaining results, it is very important to make a grid independence analysis. This tells us if the mesh used in the model is sufficiently good for the results to be trustworthy.

To obtain a trustable result out of a simulation it is very important to do a grid independence analysis. This means to improve systematically the grid of the model (using the same refinement rate for each simulation) until obtaining 3 solutions that do not reveal any new feature or behavior of the model. Moreover, each new solution must only improve asymptotically the parameter selected as a monitoring value.

In this study, two monitoring parameters are selected: the conversion of CH_4 and the selectivity of CO . The reason behind this election is that both are global parameters that depend on the entire model and they also are two of the most important ones of the model.

A *Variation%* is calculated based on two consecutive values of a parameter.

$$Variation\% = 100 \frac{Value_{i+1} - Value_i}{Value_i} \quad (139)$$

With i as a determined simulation and $i + 1$ as the next simulation done for the grid independence study.

When the variation % decreases two consecutive times and it has achieved a small enough variation, it means that the last three simulations (used for those two calculations) are in the grid independent area. The grid independence study results for this model are shown in Table 6.

Table 6: Grid independence analysis

Elements	Conversion yCH4	Conversion Variation	Selectivity CO	Selectivity Variation	Last Iteration Error	Time sim [s]
6720	0.54177	-	0.21826	-	4.50E-04	2589
13300	0.52578	-2.95%	0.22564	3.38%	3.90E-05	2165
26880	0.5272	0.27%	0.22623	0.26%	3.00E-05	4122
54150	0.52845	0.24%	0.22693	0.31%	2.40E-05	8304
107520	0.52937	0.17%	0.22733	0.18%	2.20E-05	19766

The table also shows the error on the last iteration performed by the solver on the corresponding simulation, the time taken for each simulation to converge and the number of elements of each mesh.

Moreover, the three last results of the grid independence study can be used to estimate the order of the method “p” which should be a value between³ 0.8 and 2.2. This is done using the formula

$$p \approx \frac{\log\left(\frac{\varphi_2 - \varphi_1}{\varphi_3 - \varphi_2}\right)}{\log(a)} \quad (140)$$

With “a” as the refinement rate which in this case is 1.4 ($\approx \sqrt{2}$) to increase around 2 times the number of elements from grid to grid, and $\varphi_1, \varphi_2, \varphi_3$ as the first, second and third solution respectively. Where the first has the coarser mesh and the third has the finer mesh of the grid independent results.

³ taken from professor Carlos Lange's MECE 539 lecture notes

With these information the discretization error can also be calculated using the order of the method and by adding it to the fine grid solution a better approximation can be achieved⁴

$$\epsilon_h^d = \frac{\varphi_3 - \varphi_2}{a^p - 1} \quad (141)$$

$$\varphi_{exact} = \varphi_3 + \epsilon_h^d \quad (142)$$

The results for the conversion of CH_4 and selectivity of CO are shown in the Table 7

Table 7: Results for order of the method, discretization error and exact solution

Parameter	p	Discretization error	Exact solution \approx
Conversion γ_{CH_4}	0.910996887	0.002564848	0.531934848
Selectivity CO	1.663185627	0.000533333	0.227863333

The results shown below are the ones obtained with the last simulation of the grid independency study therefore the mesh used for this results has 107520 elements.

Figure 11 shows the velocity profile, Figure 12 shows line graphs of the velocity at the centerline and the radial velocity at $z = 0.45$ meters

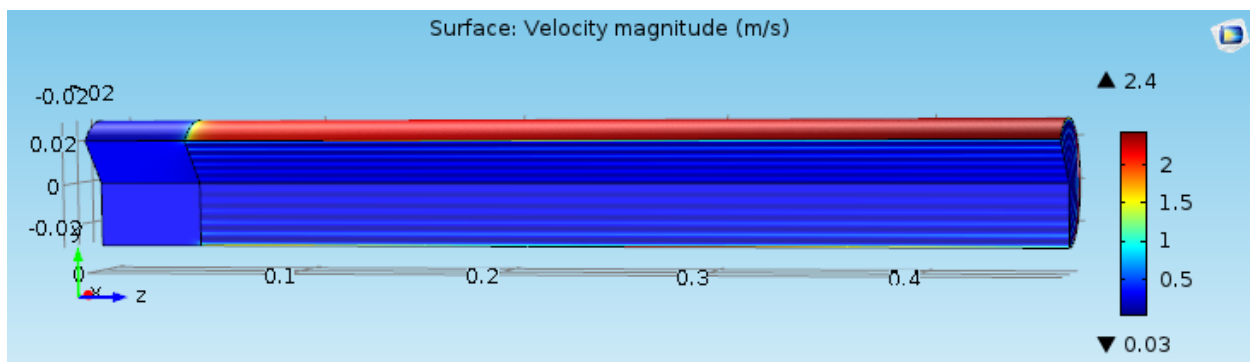


Figure 11: Velocity profile, Packed bed reactor model

⁴ taken from professor Carlos Lange's MECE 539 lecture notes

A peak in the velocity can be seen near the reactor wall. Figure 12 shows the velocity that develops axially at the center line of the reactor ($r = 0$). It is easily seen how the velocity rapidly decreases when the porous media starts (at 0.05[m]) and then it slowly increases as it approaches the outlet (at 0.47[m]). A linegraph made out of a cutline at $z = 0.45$ [m] is a good graphic representation of how the velocity behaves near the outlet.

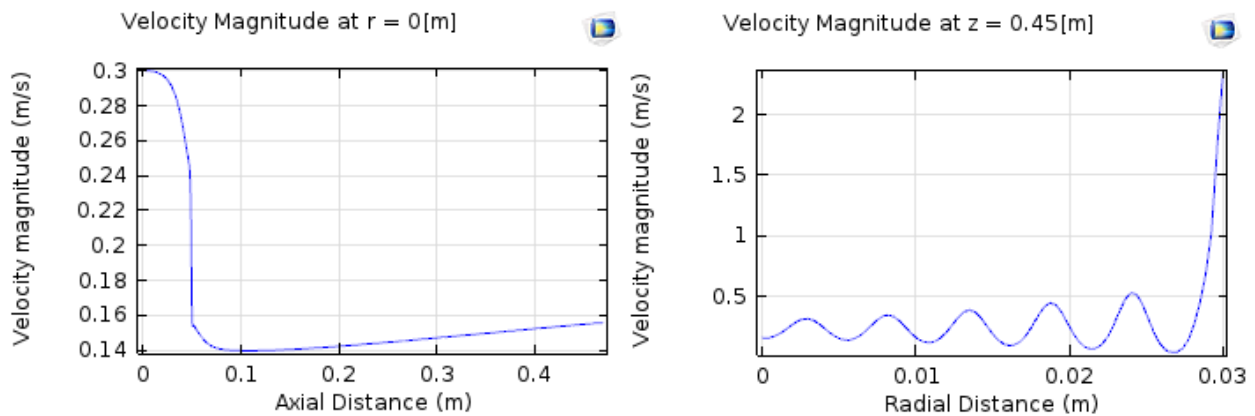


Figure 12: Axial velocity magnitude at the centerline (Left) and radial velocity magnitude at $z = 0.45$ [m]

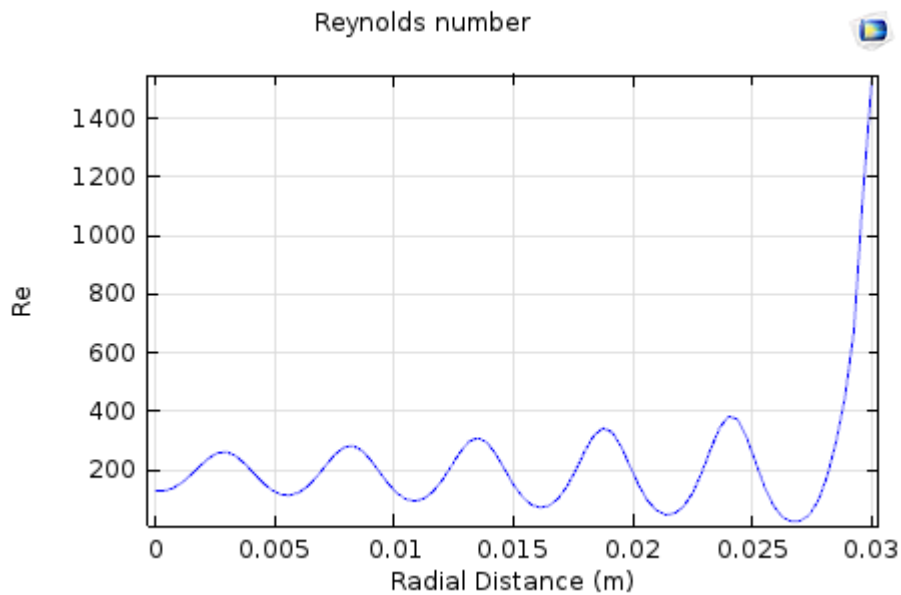


Figure 13: Reynolds number evaluated radially at $z = 0.45$ [m]

The radial behavior of the velocity is directly related with the variable porosity imposed in the model, which is constant axially but variable radially.

It can also be notice in Figure 13 that the Reynolds number goes over 1400 at the neighborhood of the wall very abruptly. This can be explained by the high velocity that the fluid has on that part of the reactor. Also, Ergun equation is only valid until a Reynolds number of about 300 but in the neighborhood of the wall the porosity tends to one which works counteracting the effect of the volume forces and Ergun equation on this part of the reactor.

The next two figures show the behavior two important physical properties: the density (Figure 14) and the pressure over the reactor (Figure 15)

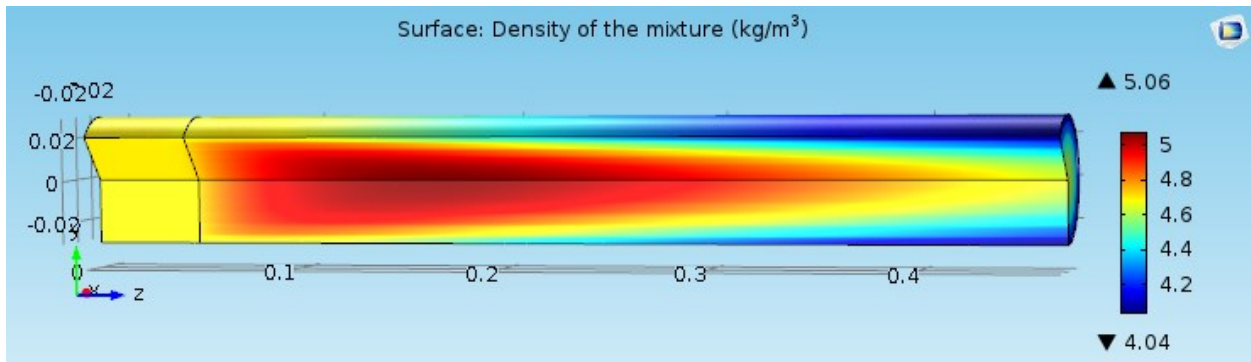


Figure 14: Density of the mixture over the reactor geometry

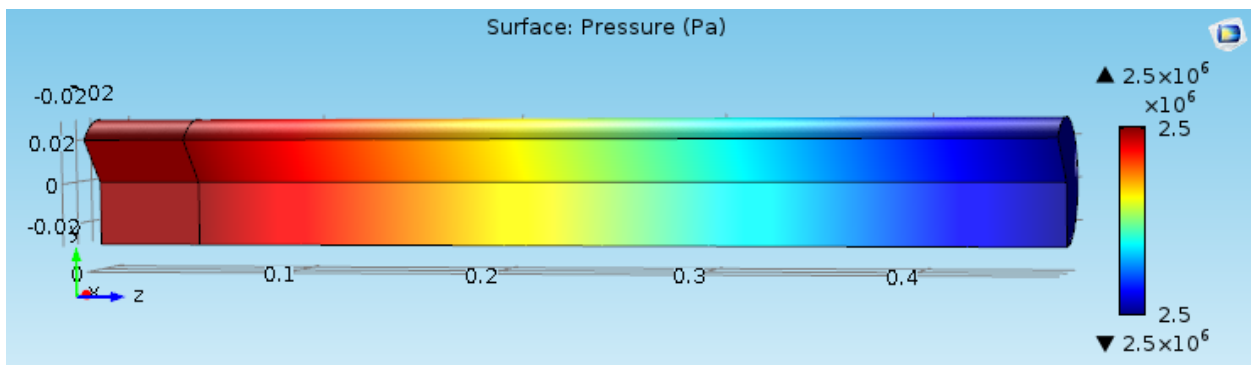


Figure 15: Pressure over the reactor geometry

The density moves between 4 and 5 kg/m³ and the pressure from 2.5006E-6 Pa to 2.5E-6 Pa

Figure 16 shows the methane mole fraction profile that is developed in the reactor.

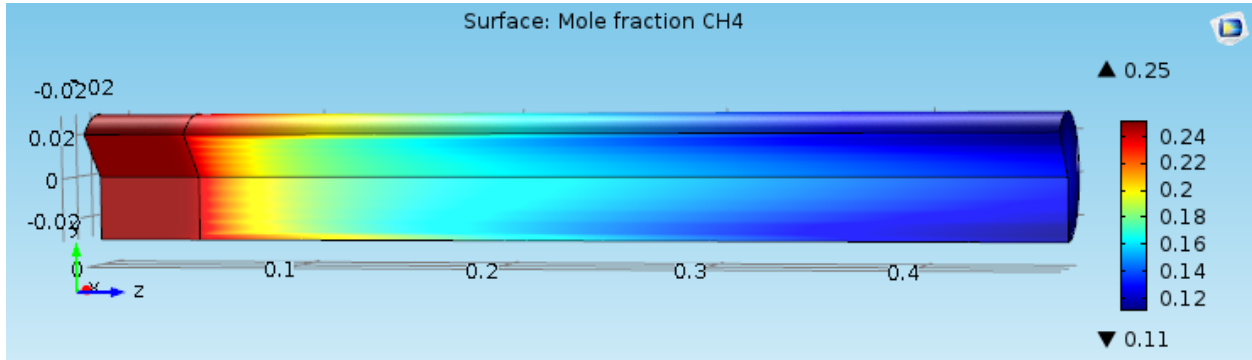


Figure 16: Mole fraction of methane over the reactor geometry

Taking the centerline of the reactor ($r = 0$) the Figure 17 shows how the mole fraction of all the components change through the reactor.

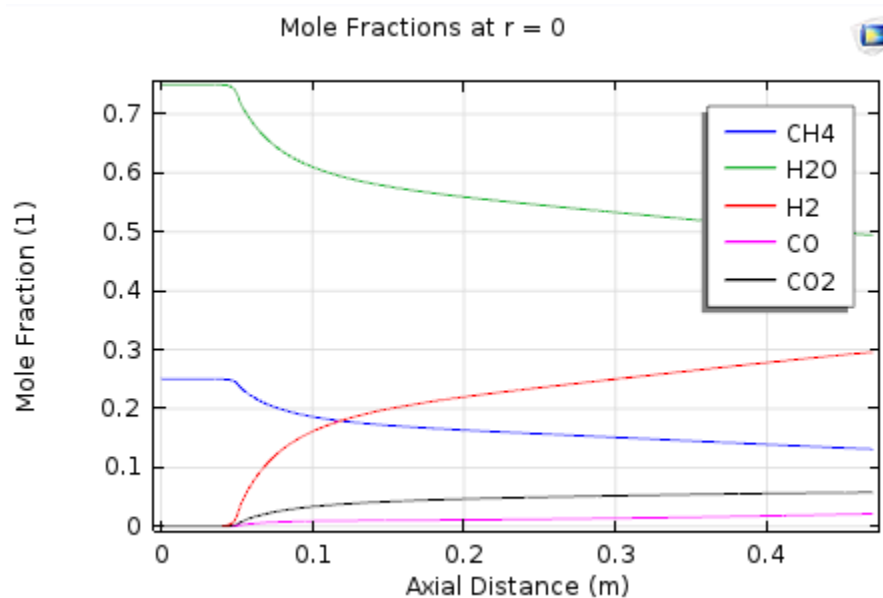


Figure 17: Axial mole fractions over the center line of the reactor

Table 8 evaluates all of the mole fractions in the inlet and in the outlet

Table 8: Comparison of the mole fractions averages over the inlet and the outlet

Mole Fractions	Inlet	Outlet
CH4	0.25	0.123
H2O	0.75	0.479
H2	0	0.313
CO	0	0.027
CO2	0	0.058

Figure 18 show the fluid temperature profile and Figure 19 shows a comparison between the fluid temperature and the solid temperature using line graphs. First on the centerline ($r = 0$) and then radially at $z = 0.45$ meters.

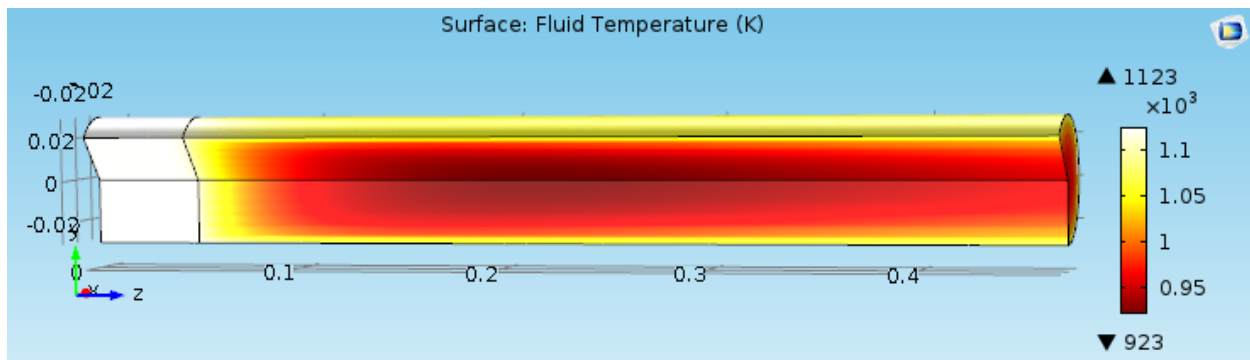


Figure 18: Temperature of the fluid over the reactor geometry

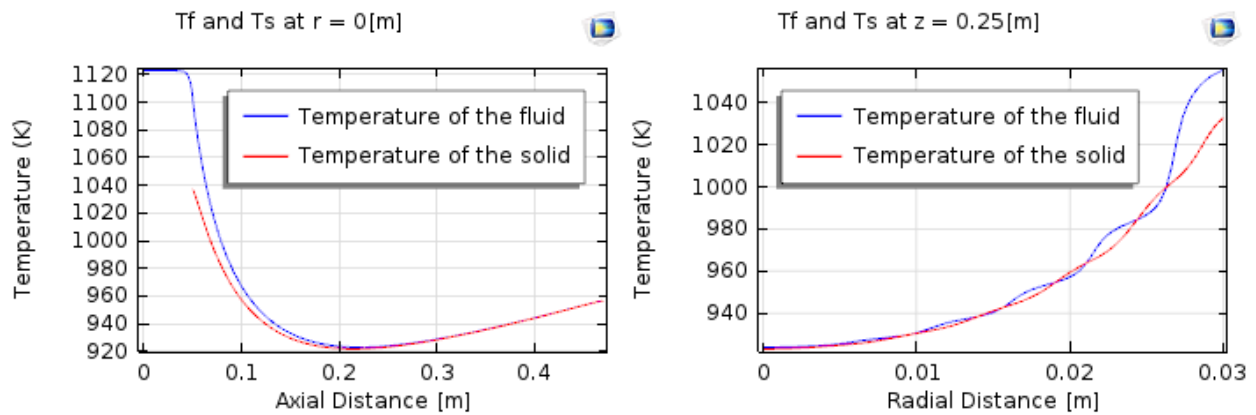


Figure 19: Comparison between the temperature of the fluid and the one of the solid.

Figure 20 shows the effectiveness factor throughout the reactor.

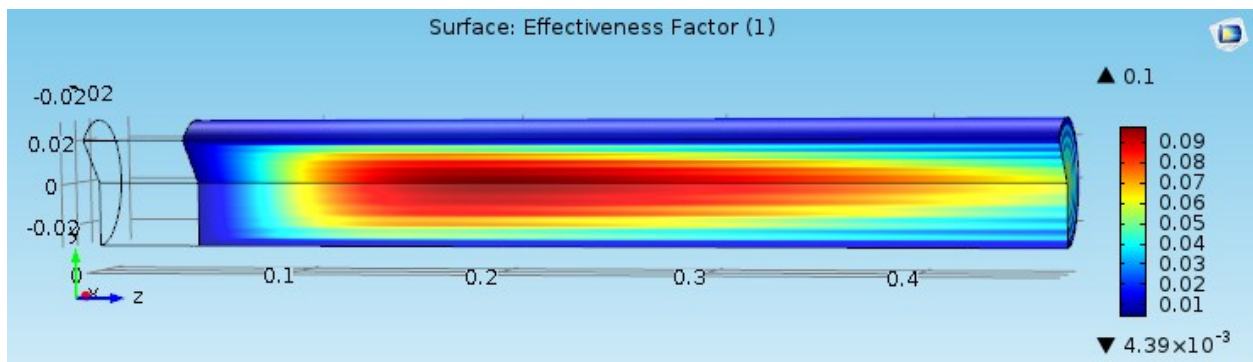


Figure 20: Effectiveness factor over the reactor geometry

Figure 21 shows the reaction rate of methane in the reactor

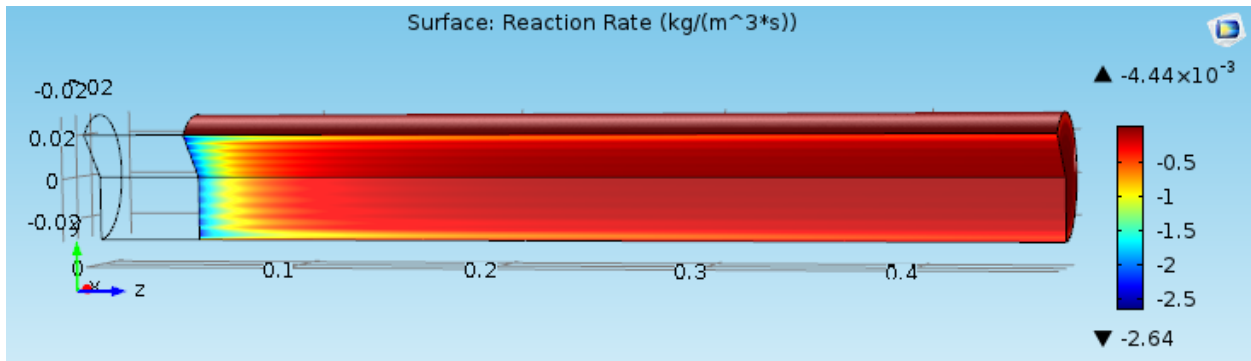


Figure 21: Reaction rate over the reactor geometry

Figure 22 is a line graph that shows the reaction rate of methane at the outlet.

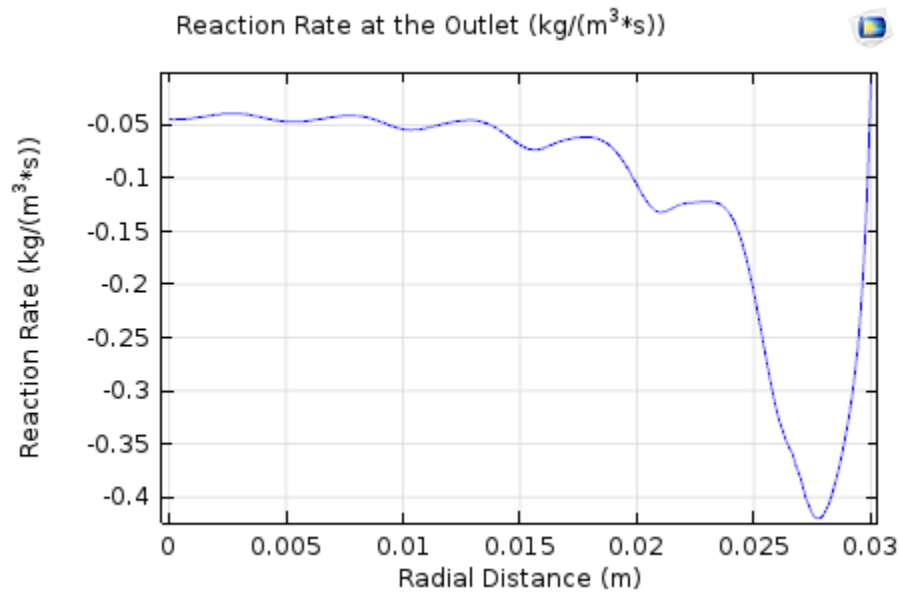


Figure 22: Radia reaction rate evaluated at the outlet

Even though very slowly, methane is still reacting at the outlet of the reactor.

4.1.1. Sensitivity analysis

The idea behind this study is to find the parameters of the model that affect the model the most. There are some parameters of this study that are related with each other. However, it is important to visualize the effect that they have because it helps to know how important is the parameter sub-model for the global model. Thus, one can keep a sub-model or look for a more accurate one in case it plays a big roll on the overall performance of the model or simply pay more attention to its behavior.

The parameters selected to be changed to evaluate their effect on the model were:

- k_{as} , axial thermal conductivity of the solid
- k_{rs} , radial thermal conductivity of the solid
- k_{af} , axial thermal conductivity of the fluid
- k_m , mass transfer coefficient
- h_{fs} , fluid-solid heat transfer coefficient
- h_{wf} , wall-fluid heat transfer coefficient
- h_{ws} , wall-solid heat transfer coefficient
- $Diff$, molecular diffusion coefficient

The study is done by multiplying one of the parameters for a constant, obtaining the data from the solution of the simulation, then going back to the original model, multiplying another parameter for a constant and so on. Each parameter was multiplied by 2 (on different simulations). $k_{as} = k_{rs}$ Which means both of them where changed at the same time (same results for both of them). However, the case when they change individually is also studied.

There are two global parameters that are chosen because of their importance to the model. This parameters are the conversion of CH_4 and the selectivity of CO , this is because both of them are very sensitive to all elements of the simulation. These are the same parameters chosen before to do the grid independence study and for the same reason.

All of the data and results obtained are compared to the original model data. In this manner, a percentage of change with respect to the original values is calculated for each parameter for each simulation. The formula to calculate this percentage is the following:

$$100 \cdot \frac{(Original\ value - Simulation\ value)}{Original\ value} \quad (143)$$

This will show the percentage on which all of the tracked values change with respect to its own original simulation value.

The results are shown in the Table 9

Table 9: Results of the sensitivity analysis of parameters of the model with its corresponding variation

Parameter multiplied by 2	Conversion CH ₄	Variation %	Selectivity CO	Variation %
Original Value	0.5272	-	0.22623	-
kas & krs	0.53765	1.98%	0.23281	2.91%
kas	0.52719	0.00%	0.22624	0.00%
krs	0.53763	1.98%	0.2328	2.90%
krs w/o direct effect on hws	0.53642	1.75%	0.23207	2.58%
krf	0.54474	3.33%	0.23704	4.78%
kaf	0.5271	-0.02%	0.22613	-0.04%
km	0.52962	0.46%	0.22712	0.39%
hfs	0.54416	3.22%	0.23657	4.57%
hwf	0.54117	2.65%	0.23473	3.76%
hws	0.5282	0.19%	0.22684	0.27%
Diff	0.52908	0.36%	0.22692	0.30%

The sensitivity analysis is done to learn more about how the parameters influence the model. From this it is found that the parameter that affects this model the most is the radial thermal conductivity of the fluid. This parameter is the one that creates the highest variation of the conversion of CH₄ with a 3.33% and the highest variation on the selectivity of CO as well with a 4.78%. The second one is the solid-fluid heat transfer coefficient with 3.22% and 4.57% respectively, and the third one is the wall-fluid heat transfer coefficient with 2.65% and 3.75% respectively.

It is also found that the parameters that affect the least this model are the axial thermal conductivity of the solid with a CH₄ conversion of 0% and a CO selectivity of 0%. It is known that the formulae for the radial and axial thermal conductivities of the solid are equal, and that is physically

impossible to increase one without the other. However, is good to easily test numerically how important the radial component of the thermal conductivity is, which would be extremely hard to measure experimentally. Other parameters that have a very small effect on the monitoring global values are the axial thermal conductivity of the fluid, the wall-solid heat transfer coefficient, the molecular diffusion coefficient and the mass transfer coefficient. In that same order starting with the axial thermal conductivity of the fluid as the closest one to zero among them.

It is actually very good news that multiplying a parameter by 2, which means a change on its value of 100% (and sometimes an effect on related parameters), at most changes the solution close to a 5%. This means that the overall model is not very sensitive and that it minimize the errors that a parameter sub-model could bring, therefore, there is no need to put a lot of effort on improving the sub-models.

4.1.2. Case studies

Table 10: Results of case studies with its corresponding variation of parameters of interest

Parameter	Standard solution	Tin =1023[K] Text=1023[K]	Variation %	vo=0.2[m/s]	Variation %	Constant Porosity =0.38	Variation %
XCH4	0.527	0.348	-34.0%	0.584	10.8%	0.570	8.0%
XH2O	0.369	0.255	-30.9%	0.403	9.1%	0.396	7.2%
yH2out	0.313	0.221	-29.3%	0.341	8.7%	0.334	6.6%
yCOout	0.026	0.010	-62.4%	0.033	26.4%	0.032	23.1%
yCO2out	0.058	0.047	-19.4%	0.059	3.0%	0.059	2.7%
SCO2	0.441	0.535	21.4%	0.410	-7.0%	0.418	-5.1%
SCO	0.226	0.125	-44.7%	0.259	14.6%	0.249	9.9%
avg η	0.020	0.061	210.7%	0.018	-5.9%	0.022	14.6%

Table 10 shows a comparison of the standard model with three cases of study. Changing these characteristics of the model changes the solution considerably but that is what one would expect. Even though the changes are expected, the interesting part is to see how the solution changes and how it affects the results of important parameters.

With X_{CH_4} as the conversion of methane, X_{H_2O} as the conversion of water steam, y_{H_2out} as the mole fraction of hydrogen in the outlet, y_{COout} as the mole fraction of carbon monoxide in the outlet, y_{CO_2out} as the mole fraction of carbon dioxide in the outlet, SCO_2 as the selectivity of carbon dioxide, SCO as the selectivity of carbon monoxide and average η as the average effectiveness factor over the reactor.

In the first case, the inlet temperature and the external temperature are reduced by 100 K. This changes the solution completely and even though the average effectiveness factor increases by 210% the conversion of methane and steam decrease by 34% and 31% respectively. One of the most affected parameters is the mole fraction of carbon monoxide at the outlet. Its value decreases in 62%.

In the second case the inlet velocity is reduced from 0.3 m/s to 0.2 m/s. In this case the conversion of methane and steam increase by 11% and 9% respectively. Also, this case increases the mole fraction in the outlet of all of the products of the reaction, highlighting an increase on carbon monoxide of 26% mostly due to an increase in on its selectivity and a decrease on the selectivity of carbon dioxide. It is curious to see that most of the parameters increase while the average effectiveness factor decreases on a 6%. However, this can be explained by the fact that because the velocity is smaller the residence time increases which means that the particles have more time to be in contact with the catalysts.

In the third case the porosity is changed from variable to constant over the reactor (0.38). In this case there is also a notable increase on the mole fraction of carbon monoxide at the outlet with a 23% due in part to the increase on its selectivity in about 10% and a 15% increase on the average effectiveness factor.

Chapter 5

5. Summary and conclusions

The main contribution of this work is the successful implementation of a variable radial porosity in a methane steam reforming process on a detailed modeled two dimensional packed bed reactor. From the studies, it can be observed how the model results differ from the ones that consider a constant porosity over the reactor which highlights its importance. Methane steam reforming is the most widespread process to obtain hydrogen-rich synthesis gas and a study of the response of the model to different stimuli is done to improve the understanding of this complex process.

A study on the main parameters used for the modeling equations is carried out to evaluate how an increase of 100% on its value affects the final result. All of the equations have errors and it is important to know how this error could affect a final model. An important conclusion of the sensitivity analysis done with the parameters, is that it is not so important to improve the existing parameters of the model because they individually have a very small contribution to the complete model.

It is important to notice in the development of this work that the principal source of the final results is the low effective diffusivities of the components of the reaction at the evaluated conditions. They are the reason why the reaction happens mostly on the surface on the catalyst particles in the one dimensional diffusion model, and this is the reason of the low effectiveness factors obtained finally over the whole reactor.

This work was completed thanks to the technology of the look-up tables, which were developed by A. Fadic.

5.1. Future work

Work related with further studies on a steam methane reforming packed bed reactor may include detailed kinetics for the development of the one dimensional diffusion model. It is worth remembering that global kinetics are used on this study for the reaction and this model is the base of the look-up tables.

In this work Ergun equation is used to account for the permeability, however, it is only valid until about a Reynolds number of 300, therefore inlet velocities higher of 0.3 m/s could not be evaluated due to the low dynamic viscosities of the components of the reaction at 25 bar. In further works other methods to account for the permeability could be used.

Also, the equation developed in this work for the variable porosity is only valid for a $D_{Tube}/D_{particle}$ ratio of 10. This means that further studies can be done for different ratios if other equations are developed for them or if a generalize equation is created.

References

- Al-Megeren, H., & Xiao, T. (2012). Natural Gas Dual Reforming. Catalyst and Process., (Advances in Natural Gas Technology).
- Benenati, R. F., & Brosilow, C. B. (1962). Void fraction distribution in beds of spheres. *AIChE Journal*, 8(3), 359–361. <http://doi.org/10.1002/aic.690080319>
- Benneker, A. H., Kronberg, A. E., Post, J. W., Ham, A. G. J. V. D., & Westerterp, K. R. (1996). Axial dispersion in gases flowing through a packed bed at elevated pressures. *Chemical Engineering Science*, 51(10), 2099–2108.
- Bey, O., & Eigenberger, G. (1997). Fluid flow through catalyst filled tubes. *Chemical Engineering Science*, 52(8), 1365–1376. [http://doi.org/10.1016/S0009-2509\(96\)00509-X](http://doi.org/10.1016/S0009-2509(96)00509-X)
- Drescher, I., Lehnert, W., & Meusinger, J. (1998). Structural properties of SOFC anodes and reactivity. *Electrochimica Acta*, 43(19-20), 3059–3068. [http://doi.org/10.1016/S0013-4686\(98\)00046-2](http://doi.org/10.1016/S0013-4686(98)00046-2)
- Eigenberger, G., & Ullmann, F. (1992). Fixed-Bed Reactors. In B. Elvers, S. Hawkins, J. F. Rounsaville, & G. Schulz (Eds.), (5th ed., p. 199). Weinheim: Wiley-VCH Verlag GmbH. Retrieved from http://books.google.ca/books?id=dgp_ngEACAAJ
- Haberman, B. A., & Young, J. B. (2004). Three-dimensional simulation of chemically reacting gas flows in the porous support structure of an integrated-planar solid oxide fuel cell. *International Journal of Heat and Mass Transfer*, 47(17-18), 3617–3629. <http://doi.org/10.1016/j.ijheatmasstransfer.2004.04.010>
- Hayes, R. E., & Mmbaga, J. P. (2012). *Introduction to Chemical Reactor Analysis* (2nd ed.). Taylor & Francis. Retrieved from <http://books.google.ca/books?id=yiQZce5uiZYC>

- Hou, K., & Hughes, R. (2001). The kinetics of methane steam reforming over a Ni/a-Al₂O₃ catalyst. *Chemical Engineering Journal*, 82(1–3), 311–328.
- Koning, G. W. (2002). *Heat and Mass Transport in Tubular Packed Bed Reactors at Reacting and Non-Reacting Conditions: Experiments and Models*. Retrieved from <http://doc.utwente.nl/38032/1/t000003e.pdf>
- Lehnert, W., Meusinger, J., & Thom, F. (2000). Modelling of gas transport phenomena in SOFC anodes. *Journal of Power Sources*, 87(1-2), 57–63. [http://doi.org/10.1016/S0378-7753\(99\)00356-0](http://doi.org/10.1016/S0378-7753(99)00356-0)
- Limbach, M., & Schunk, S. A. (2012). Acrylates from alkenes and CO₂, the stuff that dreams are made of. *Wertstoff*.
- Liu, J. A. (2006). *Kinetics, catalysis and mechanism of methane steam reforming*.
- Meisel, W. S., & Collins, D. C. (1973). Repro-Modeling: An Approach to Efficient Model Utilization and Interpretation. *IEEE Transactions on Systems, Man, and Cybernetics*, 3(4), 349–358. <http://doi.org/10.1109/TSMC.1973.4309245>
- Ming, Q., Healey, T., Allen, L., & Irving, P. (2002). Steam reforming of hydrocarbon fuels. *Catalysis Today*, 77(1–2), 51–64.
- Moulijn, J., Makkee, M., & Diepen, A. V. (2001). *Chemical Process Technology*. John Wiley & Sons Ltd.
- Nien, T., Mmbaga, J. P., Hayes, R. E., & Votsmeier, M. (2013). Hierarchical multi-scale model reduction in the simulation of catalytic converters. *Chemical Engineering Science*, 93, 362–375. <http://doi.org/10.1016/j.ces.2013.01.059>
- Richardson, J. T., & Paripatyadar, S. A. (1990). Carbon dioxide reforming of methane with supported rhodium. *Appl. Catal.*, 61(2).

- Turányi, T. (1994). Application of repro-modeling for the reduction of combustion mechanisms. *Symposium (International) on Combustion*, 25(1), 949–955.
[http://doi.org/10.1016/S0082-0784\(06\)80731-9](http://doi.org/10.1016/S0082-0784(06)80731-9)
- Turányi, T. (1994). Parameterization of reaction mechanisms using orthonormal polynomials. *Computers & Chemistry*, 18(1), 45–54. [http://doi.org/10.1016/0097-8485\(94\)80022-7](http://doi.org/10.1016/0097-8485(94)80022-7)
- Twigg, M. V. (Ed.). (1989). *Catalyst handbook* (2. ed). London: Wolfe.
- Votsmeier, M. (2009). Efficient implementation of detailed surface chemistry into reactor models using mapped rate data. *Chemical Engineering Science*, 64(7), 1384–1389.
<http://doi.org/10.1016/j.ces.2008.12.006>
- Wilke, C. R. (1950). A Viscosity Equation for Gas Mixtures. *The Journal of Chemical Physics*, 18(4), 517. <http://doi.org/10.1063/1.1747673>
- Xu, J., & Froment, G. F. (1989). Methane steam reforming, methanation and water-gas shift: I. Intrinsic kinetics. *AIChE Journal*, 35(1), 88–96. <http://doi.org/10.1002/aic.690350109>
- Zeiser, T., Lammers, P., Klemm, E., W. Li, Y., Bernsdorf, J., & Brenner, G. (2001). CFD-calculation of flow, dispersion and reaction in a catalyst filled tube by the lattice Boltzmann method. *Chemical Engineering Science*, 56(4), 1697–1704.
[http://doi.org/10.1016/S0009-2509\(00\)00398-5](http://doi.org/10.1016/S0009-2509(00)00398-5)